Review

A Brief Review of the Impact of Neutron Irradiation Damage in Tungsten and Its Alloys

Adil Wazeer [1,*], Tanner McElroy [1], Benjamin Thomas Stegman [1], Anyu Shang [1], Yifan Zhang [1], Vaibhav Singh [1], Huan Li [1], Zhongxia Shang [2], Haiyan Wang [1,3], Yexiang Xue [4], Guang Lin [5,6], Tim Graening [7], Xiao-Ying Yu [7] and Xinghang Zhang [1,*]

[1] School of Materials Engineering, Purdue University, West Lafayette, IN 47907, USA; mcelrot@purdue.edu (T.M.); bstegma@purdue.edu (B.T.S.); shanganyu0718@gmail.com (A.S.); fantonyzhang@gmail.com (Y.Z.); sing1305@purdue.edu (V.S.); li4868@purdue.edu (H.L.); hwang00@purdue.edu (H.W.)
[2] Electron Microscopy Center, Purdue University, West Lafayette, IN 47907, USA; shang19@purdue.edu
[3] School of Electrical and Computer Engineering, Purdue University, West Lafayette, IN 47907, USA
[4] Department of Computer Science, Purdue University, West Lafayette, IN 47907, USA; yexiang@purdue.edu
[5] School of Mechanical Engineering, Purdue University, West Lafayette, IN 47906, USA; guanglin@purdue.edu
[6] Department of Mathematics, Purdue University, West Lafayette, IN 47906, USA
[7] Materials Science and Technology Division, Oak Ridge National Laboratory, Oak Ridge, TN 37830, USA; graeningt@ornl.gov (T.G.); yuxiaoying@ornl.gov (X.-Y.Y.)
* Correspondence: awazeer@purdue.edu (A.W.); xzhang98@purdue.edu (X.Z.)

Abstract: Neutron irradiation poses a substantial challenge in the development and application of tungsten (W) and its alloys, predominantly in the framework of nuclear fusion and fission environments. Although W is well-acknowledged for its unique properties like its high melting temperature and higher resistance to sputtering, transmutation products, such as Re and Os, form and impact the alloy properties as a result of neutron irradiation. This transmutation effect accompanied by significant microstructure damage due to neutron irradiation can lead to the significant degradation of mechanical properties. This review surveys the literature focusing on the microstructural modifications post-irradiation and its impacts on the irradiation hardening. This review provides insights into the elaborative understanding on the neutron radiation damage on W and W alloys by exploring the microstructural evolution and hardness changes post-irradiation. The gaps and future opportunities for understanding neutron radiation damage in W are briefly summarized

Keywords: neutron; irradiation; tungsten; tungsten–rhenium; dislocation loop; precipitates; irradiation hardening

1. Introduction

Owing to its exceptional characteristics such as its ultrahigh melting temperature (>3400 °C), effective heat transfer rate, lower sputtering yield, low erosion rate via particle bombardment, and low tritium retention, tungsten (W) is considered as a promising and widely employed plasma facing material (PFM) in fusion environments [1–3]. When tungsten is exposed to neutron irradiation involving higher temperatures and heat flux, it experiences significant microstructural variations and alterations in their thermo-mechanical characteristics [4,5]. High energy neutron irradiations result in severe lattice structure damage, producing microscale and nanoscale defects like dislocation loops, voids, and precipitates [6,7]. These precipitates are often enriched with transmutation products like rhenium (Re) and osmium (Os) in W along with the formation of voids and dislocation loops [8]. With the application of increased level of neutron flux, the accretion of solid transmutation elements takes place, which further results in the transformation of pure W into W-Re, W-Re-Os, or W-Os alloys [9]. Radiation induced void swelling and precipitates can

introduce substantial irradiation hardening, the elevation of the ductile-to-brittle transition temperature (DBTT), and radiation embrittlement in W [10,11].

Tungsten shows brittle behavior at room temperature. To improve the ductility, alloying elements (Re, Os, Ti) could be incorporated. Among all solutes, Re displays better performance in reducing the DBTT of W and, thereby, improving the ductility [12]. The responses of W and its alloy to neutron exposure have been investigated extensively, seeking correlation among the temperature, dose rate, neutron flux, He bubble density, type of reactors, and neutron energy spectrum [13–15]. Several inferences have been drawn based on the existing research through microstructural investigations of the irradiated W. The testing temperature ranges from low (~300 °C) to high temperature values (>1000 °C), and dose rates ranging from as low as 0.03 to more than 4 dpa have been studied [16]. The generation of defects like voids, dislocation loops, and precipitates post-irradiation greatly depends upon the irradiation conditions.

The transmutation effects on W characteristics are quite complex. A study shows the decrement of thermal conductivity to nearly half of pure W when 5% Re is added into W [17], whereas its addition enhances the mechanical properties at high and low values of temperature [18,19]. Many research groups are engulfed in this topic since early 1980. Figure 1 shows a histogram plot displaying the neutron-irradiation-related publications since 2000 and up to mid-2024 and by specific research groups. Sikka et al. [20] studied the generation of precipitates post neutron irradiation of W. Precipitates of the χ phase (W-Re$_3$) were observed at 1000 °C in W-25%Re. Nemato and Hasegawa [21] studied the microstructural modification in W-Re under neutron irradiation. They performed a comparative study based on their previous work on W-26%Re. Different temperatures (372, 405, 518, 599, and 800 °C) were opted for irradiation in a fast flux test facility involving a JOYO reactor. The results showed the presence of χ- and σ-phase precipitates, which resulted in increased irradiation hardening and embrittlement. The irradiation-induced transmutation and corresponding effects on W are subjective to the neutron spectrum in different reactors [22–26]. Hasegawa reported the effects of the neutron irradiation of W and its alloys in different reactors, showcasing the relation and dependence of the dose rate, temperatures, and neutron energy spectrum [27,28]. Increases in precipitate and solution hardening owing to an increase in Re and Os content were discovered. A higher degree of irradiation hardening was observed in HFIR as compared to JOYO along with an upsurge in electrical resistivity in samples exposed in HFIR.
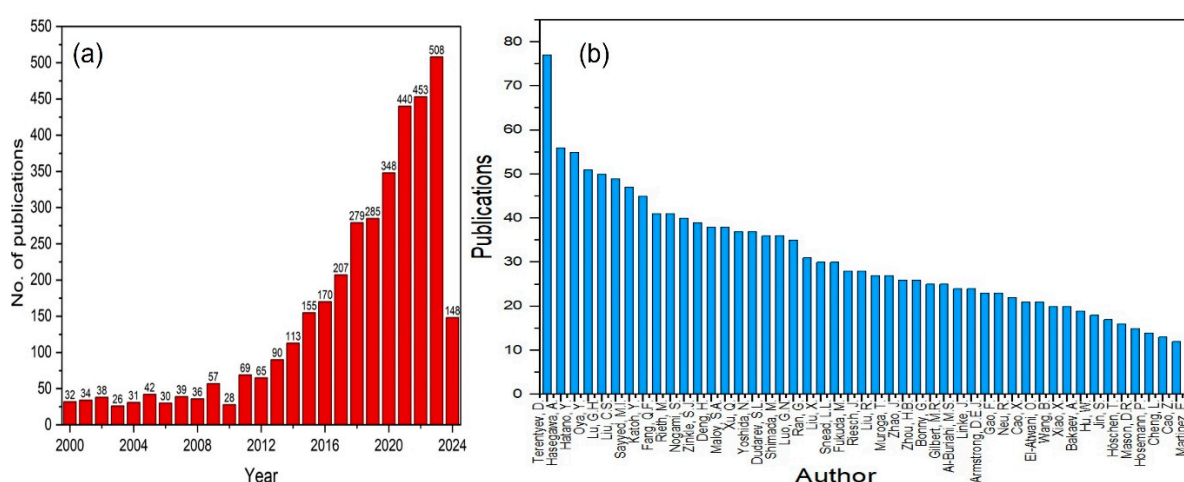

Figure 1. (**a**) Publications on the neutron irradiation of W spanning from 2000 to early 2024. (**b**) Neutron irradiation related publications over the years by several groups (as per the Scopus database).

In the present literature on the neutron irradiation of W and its alloys, limited studies are available to comprehensively evaluate the correlation between the microstructural damage (including voids, dislocation loops, and transmutation precipitates) and variations

of mechanical properties, and the influence of the energy spectrum of different reactors on such correlations. Some research groups have tried to generate defects as functions of dose rates and variations in temperature and investigate micromechanical property changes occurring in W and W alloys [29,30]. A simple methodology for the analysis of the existing literature on the neutron irradiation of the W and W-Re alloy was adopted by plotting various 2D and 3D plots of the datasets, such as the defect size and density as a function of radiation dose and temperature, obtained from the published literature in Origin software 2023. The description of each TEM image obtained from published papers was reviewed carefully and crucial TEM images were reported based on the temperature, dose, and type of reactor used to showcase a comparative examination of the material, reactor type, type of defects, and defect density. The article first reviews the microstructural changes post-irradiation by showcasing classical TEM studies on the major types of defects. This section is followed by the effects of transmutation in the W and W-Re alloys post neutron irradiation characterized by the addition and generation of Re and Os precipitates in tungsten. Further, a section is dedicated to explain the effects of neutron irradiation hardening on W and W alloys depending upon the dose, temperature, and reactor type and elaborate a detailed analysis of irradiation hardening. A comprehensive database is unavailable but it is crucial to examine the relationship between damage accumulation, damage mechanisms pertaining to fast and mixed spectrum reactors. This paper presents a corelative response of such issues and provides a damage characterization review for W and its alloys in the most widely employed reactors, namely, HFIR, JOYO, and JMTR. Moreover, the article briefly summarizes the gaps in the ongoing experimental investigations on W and its alloys.

W and W alloys are promising candidates for high-dose radiation environments, due to their exceptional characteristics as described in this section. Their radiation response directly influences their viability in environments where materials are subjected to high neutron fluxes. This review helps in assessing the formation of irradiation-induced vacancies, voids, dislocation loops, and transmutation products, and their impact on irradiation hardening and embrittlement, which influence the long-term reliability of the irradiated W and W alloys [22–25,31–33]. The subject reviewed in this study may benefit the nuclear fusion reactor sector in understanding the ability of W and W alloys to withstand extreme neutron fluxes, high heat loads, and material damage conditions critical to reactor performance and longevity. While the use of W and its alloys involves an initial investment of large capital, their longevity under neutron irradiation could offset replacement costs for critical components when using other low-cost materials, such as high-temperature ceramics, reducing lifecycle costs tied to maintenance and downtime costs in reactors. Due to lower activation levels, W alloys also produce less long-lived radioactive waste than some of the elements with high radioactivity, potentially reducing waste management costs [34].

2. Microstructural Development

Microstructural modifications in the neutron irradiated W have been widely studied [35–37]. Typical developmental microstructures characterized via transmission electron microscopy show the occurrence of voids, dislocation loops, and transmutation-induced precipitates [38–44]. Radiation-induced defect migrations in W results in the grain growth promoted by neutron flux exposure. For example, an elevation in grain sizes was observed [45] when pure W is irradiated in HFIR at 850 °C. Grain size upsurges to more than 23 μm when compared with an unirradiated sample having a grain size of 5 μm. Prior studies show that, at low dosage values (<1 dpa), voids are coupled with dislocation loops in W irradiated in almost all the reactors, i.e., HFIR, JOYO, and JMTR. The dominance of dislocation loops is observed during temperatures below 500 °C and less than 0.5 dpa. The occurrence of voids at low dose and low temperature is due to the establishment of vacancy clusters that endured the displacement cascade [46]. A comprehensive explanation of defect generation and its mechanism, along with the observed gaps in the existing

database of the neutron irradiation of W and W alloys, is presented in the forthcoming subsections. The impacts of neutron exposure in W have been investigated by employing both fast and mixed spectrum neutron reactors. Thermal neutrons result in the production of solid transmutations through neutron capture reactions. Moreover, the outcomes of such transmutations are illustrated in the following sections.

2.1. Voids

During neutron irradiation, W would experience volumetric swelling during the occurrence and growth of voids. Neutron radiation induces abundant vacancy clusters in W. These vacancy clusters evolve into voids, by a net increment in the number of vacancies absorbed over interstitials. He et al. [47] performed the neutron and proton irradiation on W and W-Re-Os alloys in JMTR. They observed more void formation in proton-irradiated samples than in the neutron-irradiated specimens. With an increase in the Re content in the W alloy, the void size is similar (i.e., ~1.2 nm) at 600 °C and 0.15 dpa, but the void density decreases by half in W-3Re as compared to W. The TEM images in Figure 2 show voids in neutron-irradiated W at different doses and temperatures in HFIR and JOYO reactors [20,29,46,48]. Hu et al. [46] performed neutron irradiation in single-crystal W at low dose and high temperature in HFIR (in Figure 2a). A low void density was observed along with the formation of dislocation loops and precipitates. These voids formed before precipitate formation. Beyond 1 dpa, the void density decreases with the appearance of acicular precipitates as seen in Figure 2b [29]. At this dose level, the density of dislocation loops reduces, accompanied by the presence of transmutation precipitates and cavity growth.
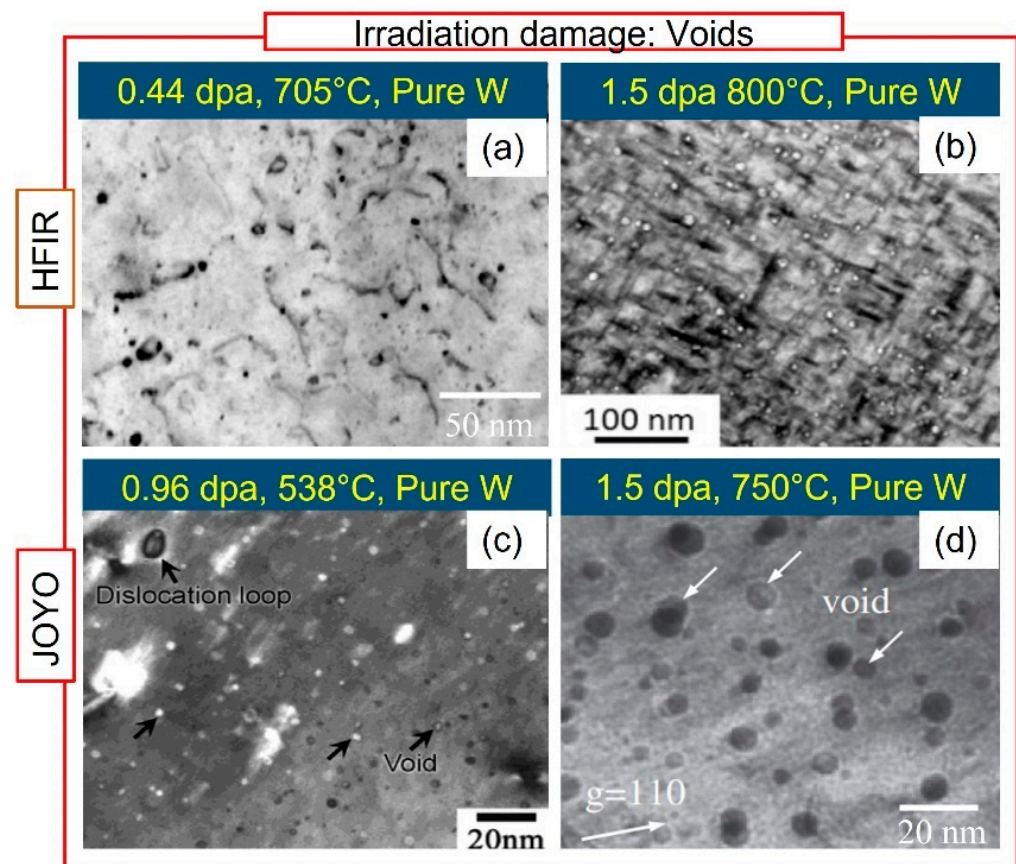

Figure 2. TEM images of voids in neutron-irradiated pure W in HFIR at (**a**) 0.44 dpa/705 °C. Reprinted with permission from Ref. [46]. 2019, Elsevier and (**b**) 1.5 dpa/800 °C. Reprinted with permission from Ref. [29]. 2019, Elsevier, and JOYO at (**c**) 0.96 dpa/538 °C. Reprinted with permission from Ref. [48]. 2016, Elsevierand (**d**) 1.5 dpa/750 °C. Reprinted from Ref. [35].

In JOYO, the void density increases with an average void size of ~2 nm below 1 dpa and temperature below 500 °C as shown in Figure 2c. Theses voids are accompanied by large dislocation loops as inferred by Fukuda et al. [48]. The authors compared experimental investigations in HFIR and found the void density for pure W is less in HFIR than in JOYO at a similar radiation dose, and ascribed the suppression of voids to the large quantity of transmutation product (precipitates) in HFIR. Tanno et al. [20] investigated the effect of the neutron irradiation of W in JOYO in the temperature range of 400 to 750 °C and above 1 dpa. At low temperatures (<500 °C) and doses (<1 dpa), densely populated nanovoids were seen along with dislocation loops, but the void size elevated as irradiation dose levels were near 1 dpa. Samples irradiated at high dose (1.5 dpa) and high temperature (750 °C) contained large voids with a diameter of 3–8 nm as shown in Figure 2d. The highest void density was observed in samples irradiated at 0.98 dpa and 538 °C.

Tanno et al. [49] studied the transmutation effects on W-Re and W-Os alloys via neutron irradiation and observed a void lattice in W irradiated at 1.54 dpa and 750 °C. The void lattice spacing and void diameter are 20 nm and 5 nm, and the alignment of lattice is along the [100] direction. Other features such as dislocation loops were found to be scarce. In the case of W-10%Re, a lower void density was observed along with few dislocation loops, and the radiation damage was dominated by needle-shaped precipitates. The voids seem to be diminished in the W-3Os alloy, although some interstitial defects (black dots) were assumed to be present.

2.2. Dislocation Loops

In irradiated BCC metals, self-interstitial atoms group to form 2D platelets enclosed by edge dislocations referred to as dislocation loops. Most of these dislocation loops have Burgers vectors of <100> and ½ <111>. <100> dislocation loops have little mobility; on the other hand, ½ <111> loops are highly mobile [50–53] and they vanish rapidly at dislocation networks and grain boundaries. The appearance of ½ <111> dislocation loops in TEM is mainly due to their trapping in their glide cylinders. Furthermore, irradiation experiments reveal the movement of these dislocation loops are often linked with solute particles [54,55]. Simulation studies show that, due to the solute–loop interactions, certain solutes offer strong binding connections with loops, leading to mobility reduction in concentrated and dilute alloys [56,57].

Fukuda et al. [58] performed the neutron irradiation in HFIR, at 500 °C and below 1 dpa in W and W-Re alloys. In W, dislocation loops were observed with a density of 3.3×10^{22} m^{-3} and size of 2.9 nm without the presence of voids, but accompanied by a high density of precipitates (Figure 3a), while, in W-5Re, the dislocation loop density increases to 5.2×10^{22} m^{-3}. The loop size remains similar to W and the precipitate density in W-5Re was 2.6×10^{23} m^{-3}. On increasing the Re content, dislocation loops diminish along with voids. At a higher dose, 2.88 dpa and 770 °C, as shown in Figure 3b, dislocation loops having an average diameter of 3.6 nm were observed with small amounts of voids; precipitate formation might have restricted the generation of voids in pure W. A dose range of more than 1 dpa reveal the effect of the neutron fluence in microstructural modifications and irradiation hardening. Fukuda et al. [59] investigated irradiation experiments with JOYO to examine the Re influence on the microstructural modifications and irradiation hardening in W. For W irradiated at 583 °C and 0.47 dpa, the void density is much higher as compared to the dislocation loop density. The diameter of voids and dislocation loops are comparable and is ~3 nm. On increasing the Re content from 3 to 5 at. % (Figure 3c), the dislocation loop density doubled as compared to pure W and the void density dropped along with a decrease in the void size and an increase in the size of dislocation loops. Void nucleation and growth occurred in W at 583 °C but was suppressed in W-Re, and, quantitatively, the void density in W-Re alloys was nearly 1/100 of that in W. Tanno et al. [49] also studied the neutron irradiation of the W-Re alloy over 400–750 °C and 0.17–1.54 dpa. A void lattice was observed at 1.54 dpa and 750 °C (Figure 3d), along with small voids and dislocation loops in W-10%Re.
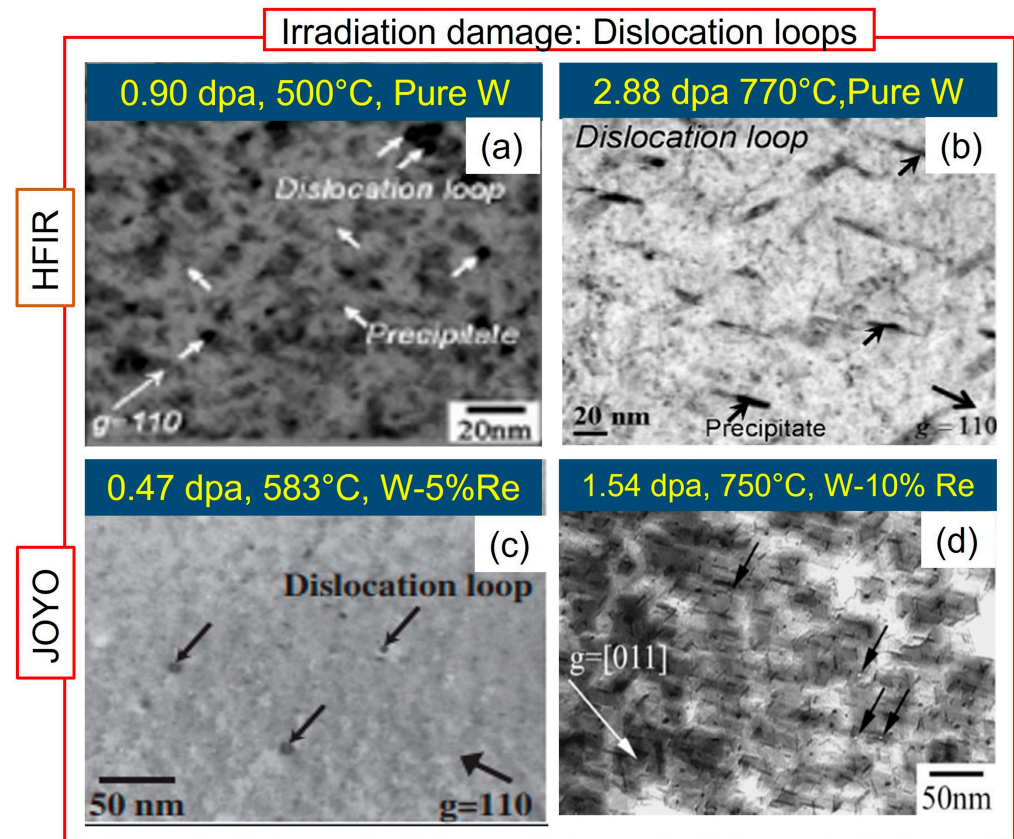
Figure 3. TEM images of dislocation loops in Pure W in HFIR at (**a**) 0.90 dpa/500 °C. Reprinted with permission from Ref. [58]. 2014, Elsevier and (**b**) 2.88 dpa/770 °C Reprinted with permission from Ref. [58]. 2014, Elsevier and in W-Re alloys irradiated in JOYO reactor at (**c**) 0.47 dpa/583 °C. Reprinted from Ref. [59] and (**d**) 1.54 dpa/750 °C. Reprinted from Ref. [49].

2.3. Transmutation-Induced Precipitates

There has been increasing studies on the transmutation-induced precipitates in W by neutron irradiation [60]. Hu et al. [46] reported the effects of transmutation in the generation of Re and Os containing precipitates in W and their dependance on the dose rate and applied temperature in HFIR. Radiated samples at low dose, 0.02 to 0.44 dpa, and at 450 °C–797 °C produce nanosized clusters rich in Os and Re; W irradiated at a higher dose reveals needle-like precipitates [46]. Large-size intergranular precipitates are visible in W [46]. Moreover, it was inferred that voids were linked with the needle-shaped precipitates [46]. This trend was also observed by Hwang et al. [61] where W and W-10%Re were neutron-irradiated below 1 dpa and at 500 °C in HFIR and JOYO. The formation of Re dominating clusters was studied via atom probe tomography (APT) and TEM. For W irradiated in a JOYO reactor, clusters enriched with Re were oriented in straight lines. The layout of these Re-rich precipitates was in accordance with the void lattice, suggesting the accumulation of Re around defect sinks, such as dislocation loops and voids [60,61].

Hasegawa et al. [62] explored the neutron irradiation on W and W-10%Re in HFIR. Fine transmutation-induced precipitates along with dislocation loops were observed (Figure 4a,b). The absence of voids was attributed to the formation of precipitates. In W-10%Re, acicular precipitates oriented along the [110] direction and black dot structures are present. Further diffraction analyses of the irradiated W and W-10% Re revealed the formation of σ (W-Re)-phase and χ (W-Re$_3$)-phase precipitates. When these W samples were irradiated at a higher temperature, 800 °C, the dimensions of the precipitates (σ- and χ-phase) increased further (Figure 4 c,d) as compared to samples irradiated at 500 °C. The types of precipitates observed in the JOYO reactor [35] are similar to those observed in HFIR. Tanno et al. [35] irradiated W-Re alloys in JOYO to infer the development of

precipitates in these alloys. Plate-shaped precipitates oriented along the {110} planes were observed and were characterized as the χ phase in W-Re alloys irradiated at 750 °C, 1.54 dpa. W-Re samples irradiated at 750 °C and 1.5 dpa reveal small black features identified as σ-phase precipitates.
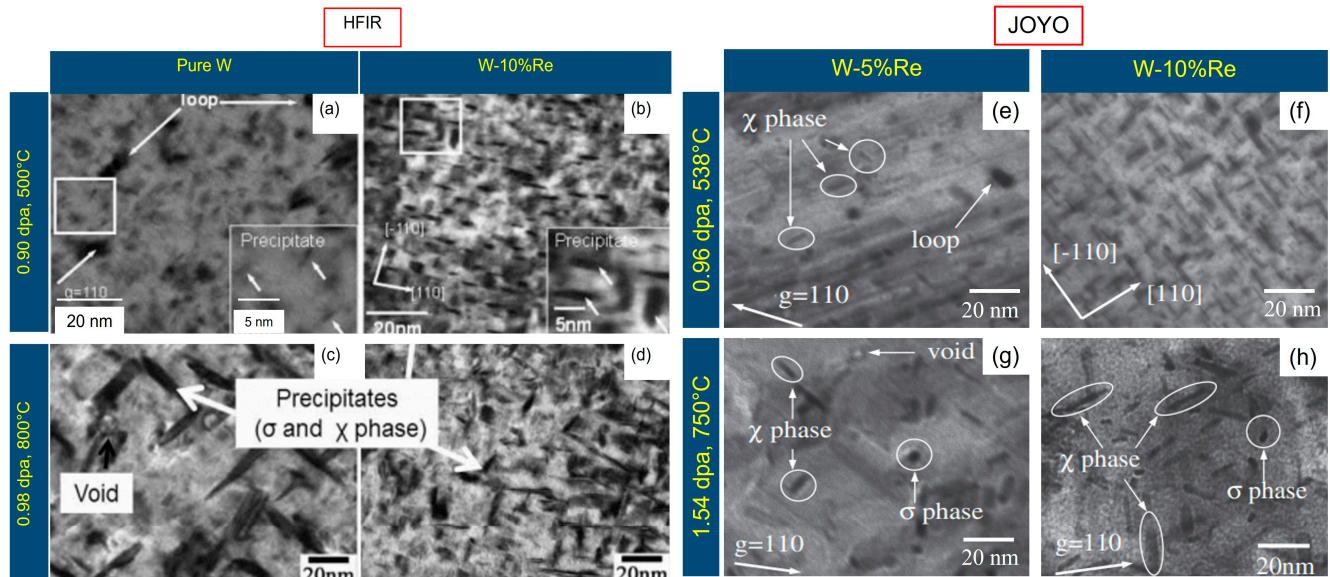

Figure 4. TEM images of precipitate formation in (**a–d**) HFIR. Reprinted with permission from Ref. [62]. 2016, Elsevier and (**e–h**) JOYO. Reprinted from Ref. [35] reactors for neutron-irradiated W and W-Re alloy.

In order to explore more deeply the precipitate formation, a study performed by Hwang et al. [61] reveal the Re cluster size observed in the TEM micrograph was higher than that experienced in APT studies for W and W-Re alloys irradiated at around 500 °C and below 1 dpa. Moreover, the number density of precipitates was lower than that of Re-rich clusters. The comparative study of APT and TEM reveal the conversion of Re clusters into precipitates containing 0.5 to 0.4% Re.

Vesti et al. [63] studied the effect of Re in the coefficient of thermal expansion (CTE) of σ and χ phases in the W-Re alloy using two approaches, the Debye–Grüneisen (DG) model and quasi-harmonic approximation (QHA). Experimental results of W and W-Re were compared with the σ and χ phases at steady Re concentrations. The authors concluded a noteworthy incongruity in CTE of σ and χ phases which might influence the thermal stress buildup at high temperatures. This incongruity increases with the increase in temperature and Re concentration in both the σ and χ phases. Neutron-irradiation-induced Re precipitates have its concentrations beyond solubility limit [64–66]. Former studies have investigated the characteristics of σ and χ phases by opting for ab initio methodologies like density functional theory for recording fracture-related characteristics and lattice site habitation [67–70].

As shown in Figure 5, the σ-phase precipitate has a tetragonal crystal structure and fits in the $P4_2/mnm$ space group; on the other hand, the χ phase has a cubic structure [68]. Both W-Re phases are stable thermodynamically over a wide range of Re concentrations. Harrison et al. [71] explored the intermetallic W-Re phases generated in the ion-irradiated W-Re alloy. The authors experimented by inducing the σ and χ phases in W-26%Re irradiated with Ne ions at 500 °C and 800 °C, at a dose level of 5 dpa. The precipitation of these σ and χ phases is correlated with the impacts of cascade energy density and ballistic mixing.
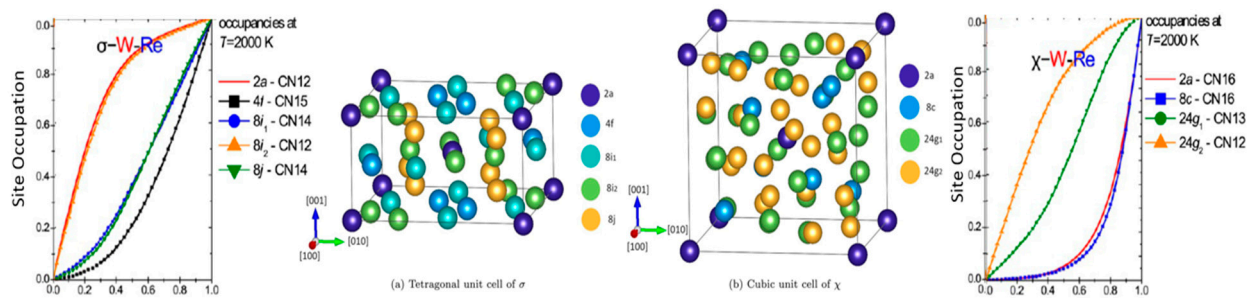
Figure 5. The crystal structure of σ (W-Re) and χ (W-Re₃) phases along with the measure of site occupancy of each phase Reprinted from Refs. [63,68].

2.4. Defect Density Variation with Temperature and Dose

Researchers have been interested in studying the correlation of the temperature and dose on the defect formation of neutron-irradiated W and W alloys. Figure 6 shows the plot of dpa vs. temperature variation generated from the datasets obtained through the existing literature on the neutron irradiation of W and W-Re alloys in HFIR, JOYO, and JMTR reactors [27–29,46,49,58–60]. Most of the data points are aggregated below 1 dpa and at ~800 °C for HFIR, although few points could be spotted beyond 1 dpa in HFIR, which are mostly for irradiated W-Re alloys (Re concentrations of 3, 5, 10, and 26 at.%), while JOYO stays put between 500–800 °C and also below 1 dpa. For the case of JMTR, the data points are found to be below 0.5 dpa and between 600–800 °C. The evident lack of data at higher dose rates, >3 dpa, discloses a gap for future studies concerning the neutron irradiation in W and W-Re alloys. The variation also corresponds to the type of reactor employed for radiation purposes. A higher dosage and temperature values are observed in HFIR when compared to JOYO and JMTR. Caution shall also be applied when comparing data among various types of reactors as the neutron spectrum can propose a significant impact upon the transmuted elements, defect generation, and mechanical characteristics of irradiated W.
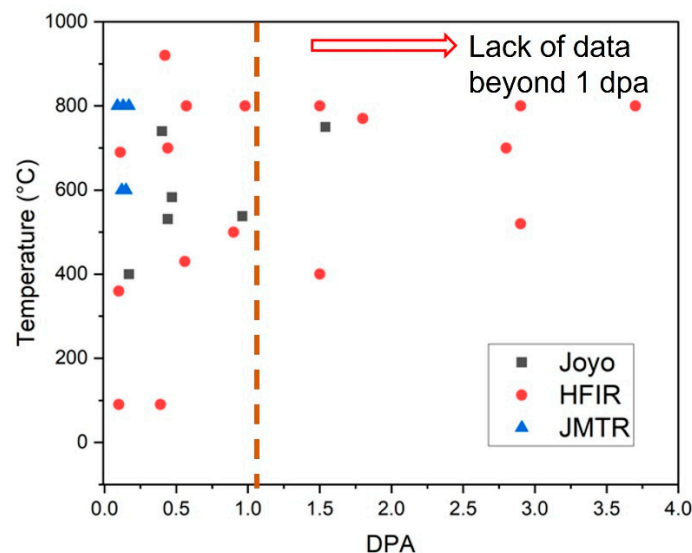

Figure 6. Plot showing variation of dpa vs. temperature in JOYO, HFIR, and JMTR reactors. Datasets obtained from references. Reused with permission from Refs. [27–29,46,58,60]. 2011, Elsevier; 2013, Elsevier; 2019, Elsevier; 2019, Elsevier; 2014, Elsevier; 2014, Elsevier. Adapted from Refs. [49,59].

The dependence of defect densities on the temperature and dose is derived from TEM studies [27–36,46,49,58–60,62], but a conclusion on the coherency of precipitates is not yet perceptible based on the limited literature datasets on the neutron irradiation of W and W

alloys. Figure 7 shows the variation of defect densities with the dose and temperature in W and W-Re alloys. The void density data are clustered below 1 dpa and show a maximum value of $1.2 \times 10^{22}/m^3$ for W in HFIR, whereas the void density for W in the JOYO reactor can be much greater at similar dose and temperature (Figure 7a). Comparing to W, the void density for irradiated W-Re alloys is much less for HFIR and JOYO reactors as shown in Figure 7b. The dislocation loop density in W in HFIR is similar to the void density in HFIR, and comparable to the loop density in W irradiated in the JOYO reactor (Figure 7c). The data scarcity for the dislocation loop density is evident for the irradiated W-Re alloy (Figure 7d). The density of irradiation-induced precipitates (containing Re and Os due to transmutation) increases with the increase in dosage (Figure 7e) and is comparable to the density of voids or loops in W. However, for the irradiated W-Re alloys, this precipitate density is nearly an order of magnitude higher than that in W (Figure 7f), having reached $80 \times 10^{22}/m^3$ for HFIR and $60 \times 10^{22}/m^3$ for JOYO. The precipitate density also increases with the greater Re concentration in the W-Re alloys. Table 1 also shows the tabulated variation of defect densities in Pure W and W-Re alloys generated from the plots shown in Figure 7. The qualitative comparison using "high" or "low" was made between irradiated W and We-Re alloys.
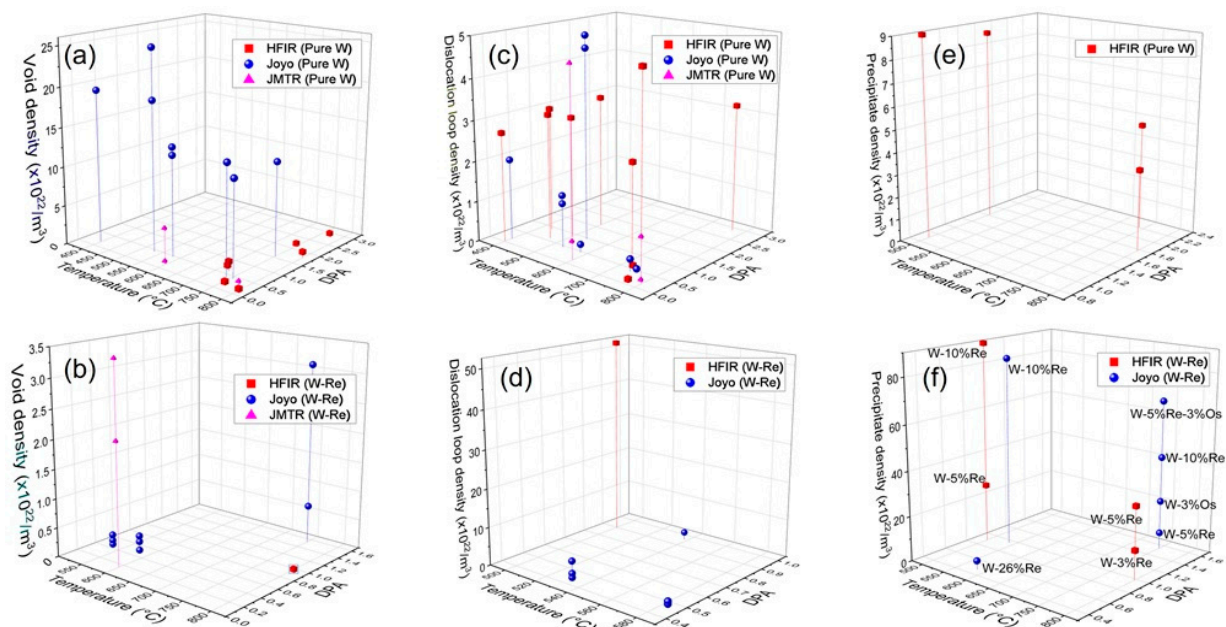

Figure 7. Variation of defect densities with dose and temperature in different reactors for W and W-Re alloys: (**a**,**b**) void density, (**c**,**d**) dislocation loop density, and (**e**,**f**) precipitate density. Datasets obtained from references. Reused with permission from Refs. [27–31,34,36,46,58,60,62]. 2011, Elsevier; 2013, Elsevier; 2019, Elsevier; 2017, Elsevier; 2022, IAEA; 2020, Elsevier; 2006, IAEA; 2019, Elsevier; 2014, Elsevier; 2014, Elsevier; 2016, Elsevier. Adapted from Refs. [32,33,35,49,59].

Dislocation loops dominate in W irradiated at temperatures below 500 °C and below 1 dpa. Cavities are also perceived above 500 °C and at a lower dose but not in abundance as compared to that at elevated temperatures. Void formation at low values of dose and temperature is a result of large cavity development [72,73]. These studies suggest that voids harmonize with dislocation loops at low dose in W in all the reactors. In some cases of W, nanoscale Re- and Os-rich precipitates were observed when irradiated in HFIR [74,75]. EDS examinations reveal that voids are arranged near precipitates [76], demonstrating that the voids offer nucleation spots for the segregation of Re and Os precipitates. At elevated levels of the irradiation dose, predominantly in W irradiated in reactors with mixed energy spectra, abundant needle-like transmutation-induced precipitates are formed. These precipitates have a high number density ($>5 \times 10^{21}/m^3$) with a length of 20 nm or

greater. For the case of polycrystalline W irradiated at 2.4 dpa, 800 °C in HFIR, notably, large W-Re-Os precipitates, exceeding 100 nm in size, were detected along grain boundaries [76]. Interestingly, many voids appeared to be highly affiliated with these precipitates. Table 2 presents the summary of the defect size and density in irradiated W and W-Re alloys in the HFIR, JOYO, and JMTR reactor along with the irradiation parameters.

Table 1. Defect densities in neutron-irradiated W and W-Re alloys [27–36,46,49,58–60,62].

Defect Density	Pure W	W-Re Alloy
Void density	$1–5 \times 10^{22}/m^3$	$0.2 \times 10^{22}/m^3$
	High	Low
Dislocation loop density	$1–5 \times 10^{22}/m^3$	$50 \times 10^{22}/m^3$
	Low	High
Precipitate density	$3–10 \times 10^{22}/m^3$	$10–80 \times 10^{22}/m^3$
	Low	High

Table 2. Irradiation parameters along with summary of microstructures of irradiated W and W-Re alloys in three reactors.

S. No.	Material	Reactor Type	Temp. (°C)	DPA	Dislocation Loop Size (nm)	Dislocation Loop Density ($\times 10^{22}/m^3$)	Void Size (nm)	Void Density ($\times 10^{22}/m^3$)	Precipitate Size (nm)	Precipitate Density ($\times 10^{22}/m^3$)	Ref.
1	Pure W	HFIR	500	0.9	2.9	3	-	-	5.7	9	
2	W-10 Re	HFIR	500	0.9		-	-	-	2.2	90	
3	W–5%Re	HFIR	500	0.9	2.4	52	-	-	1.9	26	[58]
4	W–3%Re	HFIR	800	0.98	-	-	~1	0.01	6.8	13	
5	W–5%Re	HFIR	800	0.98	-	-	~1	0.01	6.6	32	
6	Pure W	HFIR	800	0.15	2	4.8	3.9	0.2	-	-	
7	Pure W	HFIR	710	0.7	2.2	2.4	4.1	0.3	-	-	[48]
8	Pure W	HFIR	430	0.9	5.4	3.1	-	-	-	-	
9	Pure W	HFIR	770	2.88	3.6	3.2	6.3	0.3	-	-	
10	Pure W	HFIR	397	0.03	5.12	2.7	-	-	-	-	
11	Pure W	HFIR	467	0.6	5.38	3.1	-	-	-	-	
12	Pure W	HFIR	724	0.6	6.37	<0.01	3.03	1.22	-	-	
13	Pure W	HFIR	742	2.2	-	-	5.28	0.07	20	4.8	[77]
14	Pure W	HFIR	764	0.15	6.56	<0.01	3.49	0.5			
15	Pure W	HFIR	500	1.62	2.9	3.3	-	-	5.7	8.6	
16	Pure W	HFIR	800	1.77	-	-	3.8	0.8	16.3	3.6	
17	Pure W	JOYO	538	0.96	4.7	5	2.1	49			
18	W-10 Re	JOYO	538	0.96	~5	<2	-	-	6.8	84	[35]
19	Pure W	JOYO	531	0.44	7.5	1.3	1.1	19	-	-	
20	W–3%Re	JOYO	531	0.44	3.7	4.6	1.4	0.03	-	-	
21	W–5%Re	JOYO	531	0.44	2.9	1.4	1.7	0.2	-	-	
22	W-10 Re	JOYO	531	0.44	7.1	0.3	3.4	0.1	-	-	
23	Pure W	JOYO	583	0.47	~3	<0.2	3.1	12.8	-	-	[59]
24	W–3%Re	JOYO	583	0.47	2.1	1.2	1.9	0.2	-	-	
25	W–5%Re	JOYO	583	0.47	2.2	1.3	1.6	0.3	-	-	
26	W-10 Re	JOYO	583	0.47	4.5	0.6	3.9	0.05	-	-	
27	W-26% Re	JOYO	583	0.47	-	-	-	-	2.8	3.9	

Table 2. *Cont.*

S. No.	Material	Reactor Type	Temp. (°C)	DPA	Dislocation Loop		Void		Precipitate		Ref.
					Size (nm)	Density ($\times 10^{22}$/m³)	Size (nm)	Density ($\times 10^{22}$/m³)	Size (nm)	Density ($\times 10^{22}$/m³)	
28	Pure W	JOYO	400	0.17	-	-	-	-	-	-	
29	Pure W	JOYO	740	0.4	-	-	-	-	-	-	[35]
30	Pure W	JOYO	750	1.54	-	-	-	-	-	-	
31	Pure W	JOYO	750	1.54	-	-	4.7	12	-	-	
32	W-5%Re	JOYO	750	1.54	-	-	3.3	0.65	14	7.3	
33	W-10 Re	JOYO	750	1.54	-	-	1.6	3.1	9.5	42	[78]
34	W-3Os	JOYO	750	1.54	-	-	-	-	7.3	22	
35	W-5Re-3Os	JOYO	750	1.54	-	-	-	-	6.8	67	
36	Pure W	JOYO	756	0.42	5.6	0.1	2.5	12.1	-	-	[48]
37	Pure W	JOYO	538	0.96	4.7	4.7	2.1	49	-	-	
38	Pure W	JOYO	400	0.17	2.8	2.0	1.8	19.5	-	-	
39	Pure W	JOYO	531	0.44	5.4	1.1	1.3	25.3	-	-	
40	Pure W	JOYO	538	0.96	4.7	4.7	2.1	49	-	-	
41	Pure W	JOYO	583	0.47	5.4	0.2	2.4	13.8	-	-	[49,59]
42	Pure W	JOYO	740	0.4	12.2	0.3	2.9	13.8	-	-	
43	Pure W	JOYO	750	1.54	-	-	4.7	12	-	-	
44	Pure W	JOYO	756	0.42	5.6	0.1	2.5	12.1	-	-	
45	Pure W	JMTR	600	0.15	7.9 (rad.)	0.46	1.3 (rad.)	6.4	-	-	
46	W–3%Re	JMTR	600	0.15	3.6 (rad.)	0.14	1.1 (rad.)	3.4	-	-	[47]
47	W–5%Re	JMTR	600	0.15	3.2 (rad.)	0.15	1.2 (rad.)	2.1	-	-	
48	Pure W	JMTR	800	0.15	8.5	0.1	1.9	4.2	-	-	[48]
49	Pure W	JMTR	600	0.15	7.9	4.6	1.3	6.4	-	-	[36,79]
50	Pure W	JMTR	800	0.15	8.5	1.1	1.9	4.2	-	-	

3. Transmutation

There has been a transmutation effect observed post-irradiation where a change in the compositions of the W samples was detected. A study shows the relationship of transmuted products with dislocation loops and cavity formation [29]. Dislocation loops are suspected to be primarily of the interstitial type, having Burgers vectors of a/2 <111> [80–83]. Dislocation loops and cavity characteristics with respect to dose are shown in Figure 8 [29]. As can be seen, the number density of dislocation loops has attained a plateau below 2 dpa with the increase in the transmutation products.

There are substantial inconsistencies, such as scattered data corresponding to the dose and temperature in the quantifiable data for dislocation loops, observed across numerous studies inspecting W irradiated under the same or comparable circumstances. Alternatively, microstructures of the cavity typically show a time evolution characterized by an increase in size and a likely slow drop in number density with increasing dose [46].

Hasegawa et al. [62] performed the neutron irradiation studies on the W and W-10%Re alloy in HFIR and JOYO. For the case of samples irradiated in JOYO as shown in Figure 9a,b, when irradiated at 538 °C and 0.96 dpa, W converts to W-0.9Re, presenting voids in a higher population accompanied by small dislocation loops, whereas W-10Re changes to W-10.4Re-0.5Os showing precipitates oriented along the [110] direction. While, for the case of HFIR shown in Figure 9c,d, irradiated at almost similar conditions, pure W transmuted to W-9.2Re-5Os, having dislocation loops along with fine precipitates, and W-10Re became W-11.7Re-11Os, showing a higher population of acicular precipitates [62].

In comparison, for W irradiated at 1.54 dpa and a higher temperature, 750 °C, in the JOYO reactor, the void density decreases substantially (Figure 9e). Similar phenomena were observed for W and W-10Re irradiated in HFIR at a greater temperature (800 °C) and dose (0.96 dpa). The size of χ- and σ-phase precipitates is larger than in the W-5Re alloy.
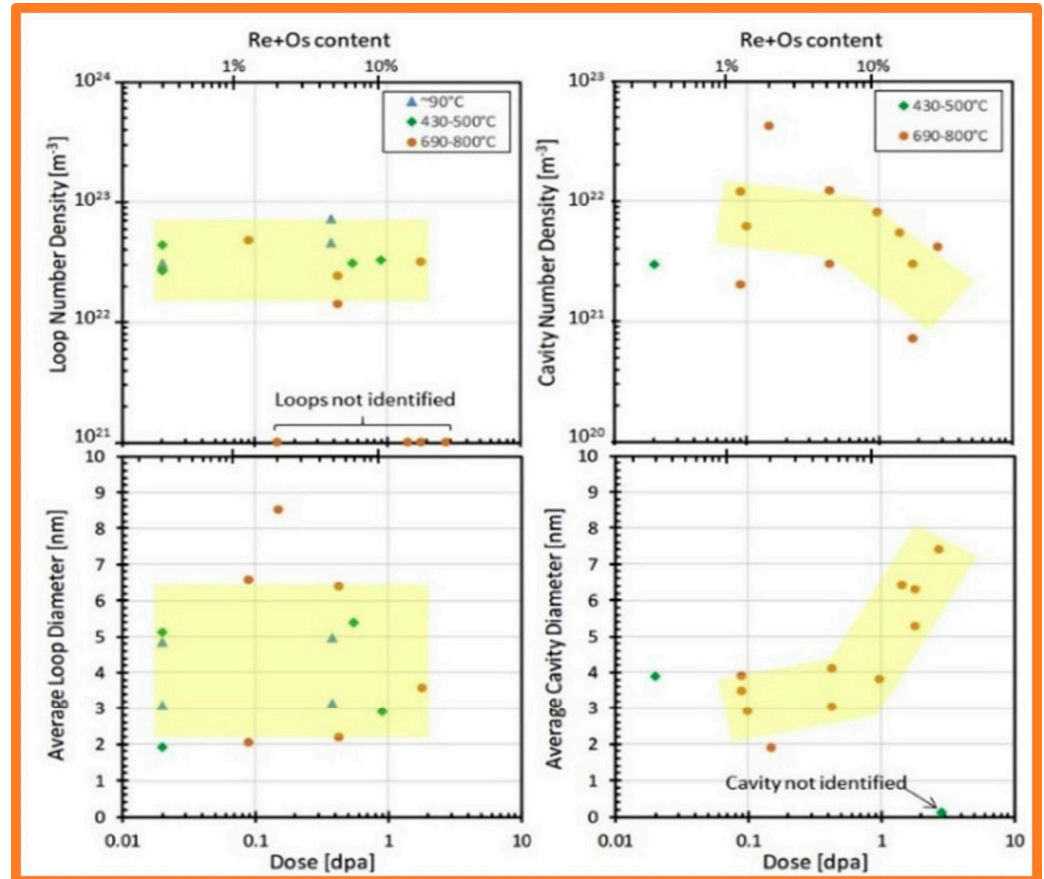

Figure 8. Dose-dependent evolution of density and diameter of dislocation loops and cavity in W during neutron irradiation in HFIR. Reprinted with permission from Ref. [29]. 2019, Elsevier. Re and Os are transmutation products in irradiated W.

Fukuda et al. [58] examined the W neutron irradiated at 1 dpa and at 800 °C in HFIR. Diffraction patterns in Figure 10a confirm the formation of the σ and χ phases. Dark-field TEM images in Figure 10c,d show that σ precipitates display an equiaxed-type structure, whereas the χ phase shows a platelet-type geometrical feature. Large precipitates were seen in pure W as compared to the irradiated W-Re alloy because of the generation of transmutation elements such as Re and Os in the matrix. The composition of W converts to W-9.22Re-5.02Os, and W-5%Re becomes W-10.46Re-8.02Os after irradiation to 0.98 dpa in HFIR. The neutron energy spectrum plays a vital role in the determination of the number of precipitates and the chemistry generated post-irradiation. For the JOYO reactor dominated by fast neutrons, transmutation is much less pronounced than in HFIR or JMTR which have much more thermal neutrons.

The segregation of transmutation elements has been performed using the STEM-EDX spectrum for neutron-irradiated W. The STEM-HAADF image in Figure 11a shows that the precipitates consist of atoms with a higher atomic number (Z) than the W matrix [84]. Bright precipitates shown in the HAADF image are identified as Os-rich features, as shown in the Os map (Figure 11b–d). Additionally, rod-shaped and spherical-shaped precipitates were also seen. The Re map further reveals an Re-enriched "cloud-like" phase surrounding the Os-rich particles (Figure 11c). Re-rich "clouds" contain an Os-rich core with a rod shape.

Additionally, few voids close to Os-rich precipitates were detected (Figure 11e–i) [84]. Transmutation-induced Os particles developed σ-WOs$_2$ and χ-WOs$_3$ precipitates with a spherical and needle-like shape, correspondingly, whereas the χ-WOs$_3$ phase is frequently observed near voids.
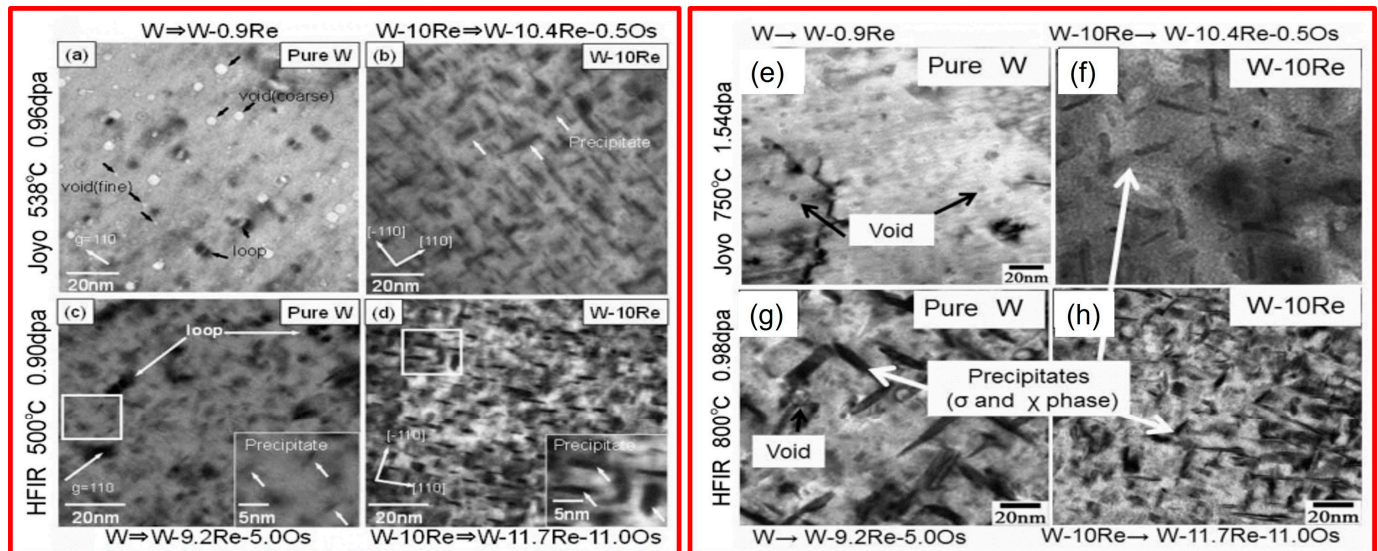

Figure 9. TEM images showing transmutation product and defect formation after neutron irradiation of Pure W and W-10%Re alloys in HFIR and JOYO reactors. Reprinted with permission from Ref. [62]. 2016, Elsevier. (**a**,**b**) W and W-10Re at 0.96 dpa/538 °C in JOYO showing voids and fine precipitates, respectively. (**c**,**d**) W and W-10Re at 0.9 dpa/500 °C in HFIR showing loops and fine precipitates. (**e**,**f**) At higher dose (1.54 dpa) and temperature (750 °C) in JOYO, void and precipitate density decrease substantially. (**g**,**h**) At 0.98 dpa and 800 °C in HFIR, precipitate density also decreases prominently.
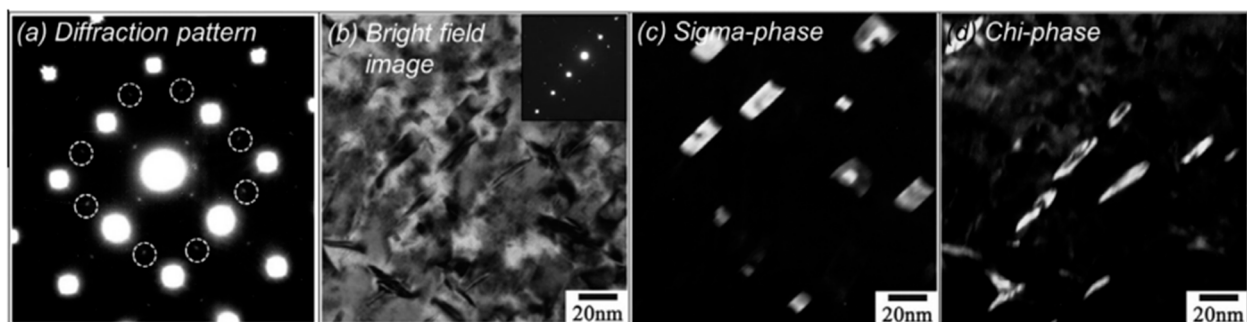
Figure 10. TEM images of W after neutron irradiation to 0.98 dpa at 800 °C in HFIR. (**a**) Diffraction pattern from [0 0 1] zone axis, (**b**) bright-field TEM image, and (**c**,**d**) dark-field TEM images of precipitates. Reprinted with permission from Ref. [58]. 2014, Elsevier.

The neutron spectrum plays a crucial role in the formation of transmutation products. It is observed that the formation of Re and Os in W is more pronounced in thermal neutron environments, as slower neutrons increase the likelihood of neutron capture reactions which convert the W to Re [85]. Fast neutron spectra reactors like JOYO may produce fewer transmutation products but induce more atomic displacements affecting the microstructural evolution [86]. HFIR allows for accelerated radiation damage, beneficial for studying the rapid accumulation of irradiation defects [87]. However, JMTR has a lower neutron flux compared to HFIR, leading to less radiation damage [88]. The intensity of neutron flux affects the rate of defect accumulation and transmutation. The high-flux HFIR reactor accelerates the formation of transmutation products and damage accumulation, which is effective for simulating long-term exposure, but also results in the increment in void

swelling and irradiation hardening [85,87,88]. This criterion is not pronounced in JMTR [88]. The JOYO reactor typically creates high energy cascades, leading to larger voids and higher levels of dislocation density than those generated in HFIR and JMTR. Thermal neutrons in HFIR and JMTR favor reactions that generate Re. A higher Re content influences the mechanical characteristics, leading to embrittlement and altering the hardening rate [88].
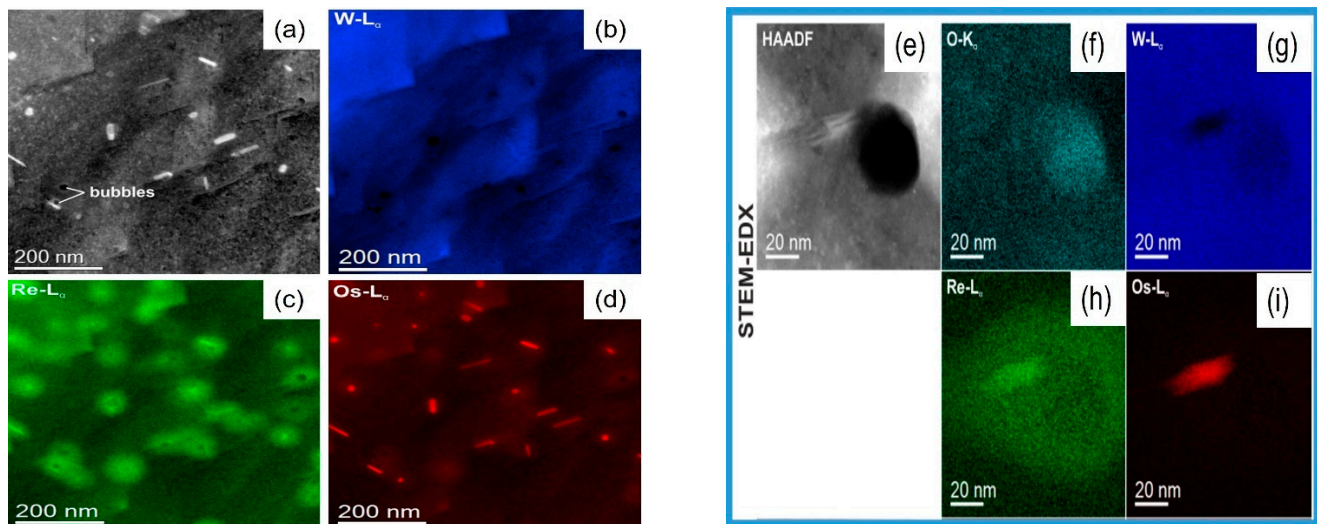

Figure 11. (**a–d**) STEM and EDX maps of W, Re, and Os near GB. (**e–i**) STEM-EDX maps of a void and a precipitate. Reprinted from Ref. [84].

4. Irradiation Hardening

Neutron irradiation induced significant microstructure damage in W and W-Re alloys; it is essential to understand the deformation mechanisms of irradiated material. This section aims to create a brief overview of the observed irradiation hardening of W and its alloys as functions of the applied dose, irradiation temperature, and reactor type.

Fukuda's group has performed various studies on the neutron irradiation effects on W and W-Re alloys [35,48,59,60,77,89,90]. One of their main findings is that the irradiation of W and W-Re alloys can be split into two main regimes. As seen in Figure 12a, regime 1 shows moderate irradiation hardening at low doses (<1 dpa), whereas regime 2 (>1 dpa) shows rapid irradiation hardening at a greater dose. Regime 1 is dominated by the formation of voids and dislocation loops as described in previous sections [48,60,77]. Although dislocation loops continue to form, Regime 2 is dominated by the formation of transmuted precipitates and is accelerated by the amount of Re present in the alloy before irradiation [35,48,59,60,77]. These precipitates inhibit the local dislocation motion, leading to the irradiation hardening as well as embrittlement. Figure 12a summarizes the irradiation hardening for two main classes of reactor, mixed spectrum reactors (JMTR and HFIR) and fast flux reactors (JOYO). Due to the differences in the neutron energy spectra in these reactors, the irradiation hardening behavior will also vary, leading to delayed precipitation in the JOYO as compared to the HFIR and JMTR [48]. In situ studies should be conducted to fully understand the interplay between void formation and the transmutation precipitation observed during the transition from Regime 1 to 2. Transmutation precipitation in Regime 2 appears to be more detrimental to the mechanical properties than the voids and loops observed in Regime 1. Figure 12b shows the relationship between the irradiation hardening and dose for W and W-Re alloys in HFIR and JMTR reactors. This comparison further acknowledges the two-regime understanding mentioned above. At Regime 1, dominated by dislocation loop and void formation, the magnitude of irradiation hardening is similar between W and W-Re alloys. At Regime 2 (>1 dpa), however, an increase in Re leads to greater irradiation hardening than W (Figure 12b). Figure 13 further emphasizes the interplay of Re in the irradiation hardening of W. At low doses (Regime 1),

the irradiation hardening observed has little dependence on the Re content. In few cases, such as at 583 °C and 0.47 dpa, irradiation softening takes place. At low doses (<1 dpa), a slight improvement in ductility was observed in the W-Re alloy (than W); however, above 1 dpa, the irradiation hardening is accelerated due to the accelerated precipitation of W into Re. Moreover, in Regime 2, Figure 13 suggests that a greater irradiation temperature leads to reduced irradiation hardening in the JOYO reactor, whereas the opposite trend was observed in HFIR-irradiated W-Re alloys. In the JOYO (fast neutron) reactor, there is limited transmutation. Greater irradiation temperatures can promote the recombination of opposite types of defects (dislocation loops and voids), and, thus, reduce irradiation hardening. However, in the HFIR reactor, higher irradiation temperatures could elevate the transmutation rate of W into Re due to excess energy, leading to a greater precipitate density, and, thus, accelerate radiation hardening [29,91].
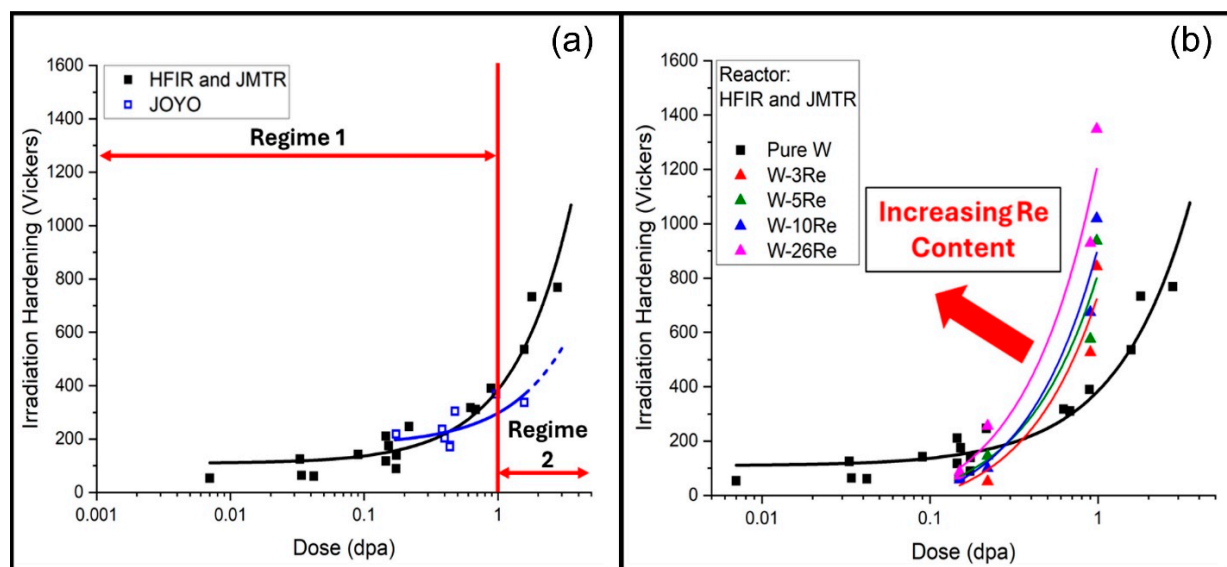

Figure 12. (**a**) Irradiation hardening vs. dose for W in HFIR, JMTR, and JOYO split into two distinct regimes. Reused with permission from Refs. [48,60,77,89,90]. 2016, Elsevier; 2014, Elsevier; 2016, Elsevier; 2020, Elsevier; 2020, Elsevier. Reprinted from Ref. [35]. Dashed line shows the predicted trend. (**b**) Irradiation hardening vs. dose for W and W- alloys in the HFIR and JMTR reactor with regime division marker. Reused with permission from Refs. [36,60,89,90]. 2006, IAEA; 2014, Elsevier; 2020, Elsevier; 2020, Elsevier. Reprinted from Refs. [35,59].

Figure 14a shows the irradiation hardening data for various doses and irradiation temperatures from the literature for W. Two knowledge gaps in terms of the lack of irradiation hardening data are identified: firstly, for high temperatures (800–1000 °C) at all doses, and, secondly, for low temperatures (<400 °C) and nearly all doses. A previous study [92,93] has focused on pure W concerning its ductile-to-brittle transition temperature, which occurs between 300–650 °C depending upon the chemistry and processing method. Significant progress has been made in characterizing the three primary types of defects, namely, voids, dislocation loops, and transmutation-induced precipitates, as evidenced by the continuous publications from major research groups around the globe [94–108]. There are ample opportunities to improve our understanding of radiation hardening in W by filling in the gaps.
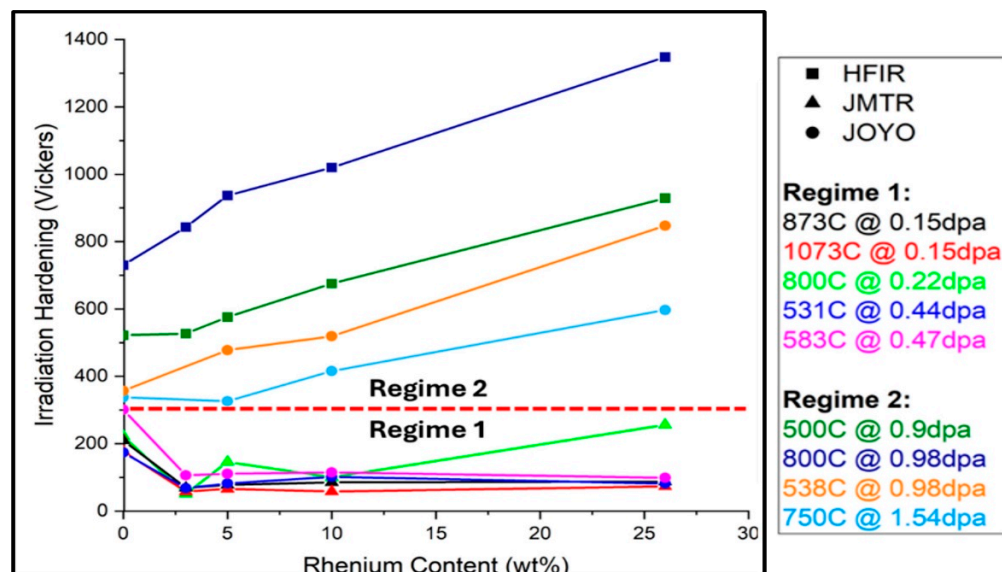
Figure 13. The influence of Re concentration on irradiation hardening of W and W alloys in different reactors. Red dashed line indicates boundary between Regimes 1 and 2. Color code corresponds to sample irradiation conditions. Reused with permission from Refs. [36,60,89,90]. 2006, IAEA; 2014, Elsevier; 2020, Elsevier; 2020, Elsevier. Reprinted from Refs. [35,59].
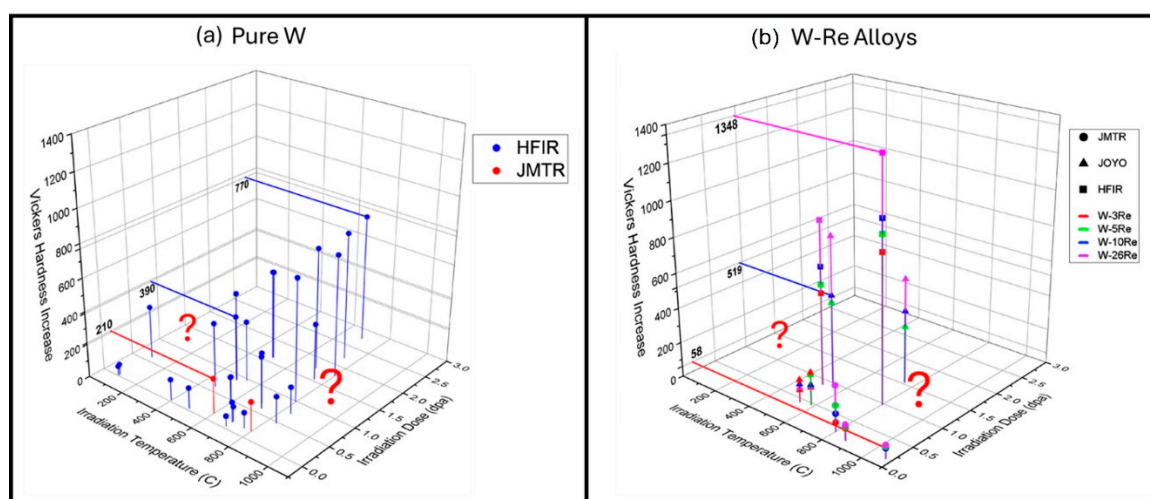

Figure 14. (**a**) 3D plot showing the dependence of irradiation hardening on irradiation temperature and dose for W in the HFIR and JMTR reactors. Reused with permission from Refs. [48,60,77,89,90]. 2016, Elsevier; 2014, Elsevier; 2016, Elsevier; 2020, Elsevier; 2020, Elsevier. Reprinted from Ref. [35]. The question marks indicate a lack of literature data in different portions of the plot. (**b**) Irradiation hardening vs. irradiation temperature and dose for W-Re alloys in the HFIR, JMTR, and JOYO reactors. Reused with permission from Refs. [36,60,89,90]. 2006, IAEA; 2014, Elsevier; 2020, Elsevier; 2020, Elsevier. Reprinted from Refs. [35,59].

Figure 14b shows the irradiation hardening behavior for W-Re alloys at different doses and irradiation temperatures. At low doses, for all temperatures, no clear trend between the Re content and the irradiation hardening could be intercepted; however, at around 1 dpa, as the Re content increases, the measured hardness difference also shows a rise in its value. The maximum hardness increase observed in Regime 1, below 1 dpa, in Figure 14b is ~400 HV, whereas the maximum hardening in Regime 2 reaches 1348 HV for the same irradiation temperature, 800 °C. This behavior further supports the claim of a two-regime understanding of irradiation hardening in W-Re alloys. Figure 14b also

highlights opportunities for furthering our understanding of radiation hardening at (1) high irradiation temperatures (800–1000 °C) and all doses and (2) low irradiation temperatures (<400 °C) and all doses. The irradiation hardening has clearly shown two regimes, low dose (<1 dpa) and high dose (>1 dpa), where radiation hardening is controlled by dislocation loops and voids at low dose, and precipitates induce significant hardening at high doses. The temperature- and dose-dependent radiation hardening have been investigated and gaps were identified at both high temperatures and low temperatures [109–127].

In order to better correlate the irradiation hardening with defect formation and the microstructural changes occurring in W and W alloys, a dispersed barrier hardening model [128,129] could be employed:

$$\Delta\sigma = M\alpha b \sqrt{\rho} \tag{1}$$

$\Delta\sigma$ is the increase in yield stress, which correlates with the hardness, M is the Taylor factor, α is the obstacle strength factor, μ is the shear modulus of the material, b is the magnitude of the Burgers vector, and ρ is the defect density.

This model suggests that irradiation hardening increases with an increase in the generation of defects due to the resistance in dislocation motion within the material lattice. The model quantitatively related the irradiation hardening increment to the irradiation-induced defect density. In W alloys, neutron irradiation induces the clustering of transmutation products, such as Re- and Os-rich clusters [14]. These transmuted defect clusters act as a dislocation barrier to the dislocation motion, contributing to hardening. A higher Re content could increase the hardness due to the solid solution hardening and precipitation hardening effects [14,15].

5. Summary and Future Outlook

This brief review highlights the current experimental surveys of W irradiated by neutrons in three nuclear reactors, focusing on the microstructure development and irradiation hardening of W and W-Re alloys. From the limited data reported so far, it is difficult to obtain a reliable prediction on the evolution of the chemistry, density, and size of Re- and Os-rich precipitates with respect to the change in temperature and at high dpa levels. Furthermore, the difference in the generation of defects (size and density of voids, dislocation loops, and precipitates) from various reactors, and their correlation with void swelling and radiation fluence remain elusive. In-depth studies on the loop nature, vacancy vs. interstitial loops, their Burgers vector, etc. are necessary in order to improve our understanding on the generation and evolution of defect clusters. Temperature- and dose-dependent variations of the loop density, defect mobility, and activation energy are critical aspects to be uncovered in order to have a comprehensive understanding of the neutron radiation damage in W and W alloys. At low doses (<1 dpa), voids and dislocation loops are prevalent in irradiated W and W-Re alloys. However, beyond 1 dpa, transmutation-induced precipitates dominate. Subsequently, the irradiation hardening varies prominently in the two regimes (low dose vs. high dose). The interplay among dislocation loops, voids, and precipitates requires further investigations. The chemical composition and crystal structure of precipitates and the mechanism for the formation and evolution of precipitates with the irradiation dose and temperature should be investigated further. Moreover, variations of the neutron spectrum (for different reactors), temperature, and dose rate also have a profound impact on defect evolutions.

Author Contributions: Conceptualization, A.W., T.M., X.-Y.Y. and X.Z.; Methodology, A.W. and T.M.; software, A.W., T.M., V.S., H.L. and Z.S.; validation, A.W., T.M., B.T.S., A.S., Y.Z., V.S., H.L., Z.S., H.W., Y.X., G.L., T.G., X.-Y.Y. and X.Z.; formal analysis, A.W., T.M., B.T.S., A.S., Y.Z., V.S., H.L. and Z.S.; investigation, A.W., T.M., B.T.S., A.S. and Y.Z.; resources, A.W., T.M., B.T.S., A.S., Y.Z., Z.S., H.W., Y.X., G.L., T.G., X.-Y.Y. and X.Z.; data curation, A.W. and T.M.; writing—original draft preparation, A.W. and T.M.; writing—review and editing; A.W., T.M., X.-Y.Y. and X.Z.; visualization, A.W., T.M., B.T.S., A.S., Y.Z., V.S., H.L. and Z.S.; supervision, Z.S., H.W., Y.X., G.L., T.G., X.-Y.Y. and X.Z.; project

References

1. Federici, G.; Skinner, C.H.; Brooks, J.N.; Coad, J.P.; Grisolia, C.; Haasz, A.A.; Hassanein, A.; Philipps, V.; Pitcher, C.; Roth, J.; et al. Plasma-material interactions in current tokamaks and their implications for next step fusion reactors. *Nucl. Fusion* **2001**, *41*, 1967. [CrossRef]
2. Wurster, S.; Baluc, N.; Battabyal, M.; Crosby, T.; Du, J.; García-Rosales, C.; Hasegawa, A.; Hoffmann, A.; Kimura, A.; Kurishita, H.; et al. Recent progress in R&D on tungsten alloys for divertor structural and plasma facing materials. *J. Nucl. Mater.* **2013**, *442*, S181–S189.
3. Rieth, M.; Dudarev, S.L.; De Vicente, S.G.; Aktaa, J.; Ahlgren, T.; Antusch, S.; Armstrong, D.; Balden, M.; Baluc, N.; Barthe, M.-F.; et al. Recent progress in research on tungsten materials for nuclear fusion applications in Europe. *J. Nucl. Mater.* **2013**, *432*, 482–500. [CrossRef]
4. Bolt, H.; Barabash, V.; Krauss, W.; Linke, J.; Neu, R.; Suzuki, S.; Yoshida, N.; Asdex Upgrade Team. Materials for the plasma-facing components of fusion reactors. *J. Nucl. Mater.* **2004**, *329*, 333–366. [CrossRef]
5. Yang, X.; Qiu, W.; Chen, L.; Tang, J. Tungsten–potassium: A promising plasma-facing material. *Tungsten* **2019**, *1*, 141. [CrossRef]
6. Arshad, K.; Ding, D.; Wang, J.; Yuan, Y.; Wang, Z.; Zhang, Y.; Zhou, Z.J.; Liu, X.; Lu, G.H. Surface cracking of tungsten-vanadium alloys under transient heat loads. *Nucl. Mater. Energy* **2015**, *3*, 4–32. [CrossRef]
7. Yang, X.L.; Chen, L.Q.; Qiu, W.B.; Song, Y.Y.P.; Tang, Y.; Cui, X.D.; Liu, C.S.; Jiang, Y.; Zhang, T.; Tang, J. Irradiation hardening behaviors of tungsten–potassium alloy studied by accelerated 3-MeV W2+ ions. *Chin. Phys. B* **2020**, *29*, 046102. [CrossRef]
8. Echols, J.R.; Garrison, L.M.; Reid, N.; Parish, C.M.; Hasegawa, A.; Bhattacharya, A.; Zhong, W.; Morrall, D.; Lance, M.; Katoh, Y. Degradation of electrical resistivity of tungsten following shielded neutron irradiation. *Acta Mater.* **2023**, *257*, 119025. [CrossRef]
9. Noda, T.; Fujita, M.; Okada, M. Transmutation and induced radioactivity of W in the armor and first wall of fusion reactors. *J. Nucl. Mater.* **1998**, *258*, 934–939. [CrossRef]
10. Matolich, J.; Nahm, H.; Moteff, J. Swelling in neutron irradiated tungsten and tungsten-25 percent rhenium. *Scr. Metall.* **1974**, *8*, 837–841. [CrossRef]
11. Rau, R.C.; Ladd, R.L.; Moteff, J. Voids in irradiated tungsten and molybdenum. *J. Nucl. Mater.* **1969**, *33*, 324–327. [CrossRef]
12. Mutoh, Y.; Ichikawa, K.; Nagata, K.; Takeuchi, M. Effect of rhenium addition on fracture toughness of tungsten at elevated temperatures. *J. Mater. Sci.* **1995**, *30*, 770–775. [CrossRef]
13. Chauhan, A.; Yuan, Q.; Litvinov, D.; Gaganidze, E.; Schneider, H.C.; Terentyev, D.; Aktaa, J. Effect of temperature on the neutron irradiation-induced cavities in tungsten. *Philos. Mag.* **2022**, *102*, 1665–1683. [CrossRef]
14. Nguyen-Manh, D.; Wróbel, J.S.; Klimenkov, M.; Lloyd, M.J.; Messina, L.; Dudarev, S.L. First-principles model for voids decorated by transmutation solutes: Short-range order effects and application to neutron irradiated tungsten. *Phys. Rev. Mater.* **2021**, *5*, 065401. [CrossRef]
15. Li, X.Y.; Zhang, Y.G.; Xu, Y.C.; Wu, X.B.; Kong, X.S.; Wang, X.P.; Fang, Q.-F.; Liu, C.-S. Interaction of radiation-induced defects with tungsten grain boundaries at across scales: A short review. *Tungsten* **2020**, *2*, 15–33. [CrossRef]
16. El-Guebaly, L.; Sawan, M. Consequences of Neutron Energy Spectrum on Radiation Damage, Gas Production, and Transmutations in Fusion Materials. *Fusion Sci. Technol.* **2023**, *79*, 932–940. [CrossRef]
17. Fujitsuka, M.; Tsuchiya, B.; Mutoh, I.; Tanabe, T.; Shikama, T. Effect of neutron irradiation on thermal diffusivity of tungsten–rhenium alloys. *J. Nucl. Mater.* **2000**, *283*, 1148–1151. [CrossRef]
18. Makarov, P.; Povarova, K. Development of tungsten-based vacuum melted and powder structural alloys. *Int. J. Refract. Metals Hard Mater.* **2002**, *20*, 277–285. [CrossRef]
19. Rau, R.C.; Moteff, J.; Ladd, R.L. Comparison of microstructure with mechanical properties of irradiated tungsten. *J. Nucl. Mater.* **1967**, *24*, 164–173. [CrossRef]

20. Sikka, V.K.; Moteff, J. Identification of α-Mn crystal structure in neutron irradiated W-Re alloy. *Metall. Mater. Trans. B* **1974**, *5*, 1514–1517. [CrossRef]

21. Nemoto, Y.; Hasegawa, A.; Satou, M.; Abe, K. Microstructural development of neutron irradiated W–Re alloys. *J. Nucl. Mater.* **2000**, *283*, 1144–1147. [CrossRef]

22. Yin, C.; Terentyev, D.; Dubinko, A.; Zhang, T.; Wirtz, M.; Antusch, S.; Petrov, R.H.; Pardoen, T. Impact of neutron irradiation on hardening of baseline and advanced tungsten grades and its link to initial microstructure. *Nucl. Fusion* **2021**, *61*, 066012. [CrossRef]

23. Dellis, S.; Xiao, X.; Terentyev, D.; Mergia, K.; Krimpalis, S.; Bakaev, A.; Messoloras, S. Mechanical properties of neutron-irradiated single crystal tungsten W (100) studied by indentation and FEM modelling. *J. Nucl. Mater.* **2021**, *551*, 152985. [CrossRef]

24. Dubinko, A.; Terentyev, D.; Yin, C.; Van Renterghem, W.; Rossaert, B.; Rieth, M.; Zhurkin, E.; Zinovev, A.; Chang, C.; Van Dyck, S.; et al. Microstructure and hardening induced by neutron irradiation in single crystal, ITER specification and cold rolled tungsten. *Int. J. Refract. Met. Hard Mater.* **2021**, *98*, 105522. [CrossRef]

25. Nogami, S.; Terentyev, D.; Zinovev, A.; Yin, C.; Rieth, M.; Pintsuk, G.; Hasegawa, A. Neutron irradiation tolerance of potassium-doped and rhenium-alloyed tungsten. *J. Nucl. Mater.* **2021**, *553*, 153009. [CrossRef]

26. Taylor, C.N.; Shimada, M.; Watkins, J.M.; Hu, X.; Oya, Y. Neutron irradiated tungsten bulk defect characterization by positron annihilation spectroscopy. *Nucl. Mater. Energy* **2021**, *26*, 100936. [CrossRef]

27. Hasegawa, A.; Tanno, T.; Nogami, S.; Satou, M. Property change mechanism in tungsten under neutron irradiation in various reactors. *J. Nucl. Mater.* **2011**, *417*, 491–494. [CrossRef]

28. Fukuda, M.; Hasegawa, A.; Tanno, T.; Nogami, S.; Kurishita, H. Property change of advanced tungsten alloys due to neutron irradiation. *J. Nucl. Mater.* **2013**, *442*, S273–S276. [CrossRef]

29. Katoh, Y.; Snead, L.L.; Garrison, L.M.; Hu, X.; Koyanagi, T.; Parish, C.M.; Edmondson, P.; Fukuda, M.; Hwang, T.; Tanaka, T.; et al. Response of unalloyed tungsten to mixed spectrum neutrons. *J. Nucl. Mater.* **2019**, *520*, 193–207. [CrossRef]

30. Koyanagi, T.; Kumar, N.K.; Hwang, T.; Garrison, L.M.; Hu, X.; Snead, L.L.; Katoh, Y. Microstructural evolution of pure tungsten neutron irradiated with a mixed energy spectrum. *J. Nucl. Mater.* **2017**, *490*, 66–74. [CrossRef]

31. Terentyev, D.; Jenus, P.; Sal, E.; Zinovev, A.; Chang, C.C.; Garcia-Rosales, C.; Kocen, M.; Novak, S.; Van Renterghem, W. Development of irradiation tolerant tungsten alloys for high temperature nuclear applications. *Nucl. Fusion* **2022**, *62*, 086035. [CrossRef]

32. Vrielink, M.O.; Shah, V.; Van Dommelen, J.A.W.; Geers, M.G. Modelling the brittle-to-ductile transition of high-purity tungsten under neutron irradiation. *J. Nucl. Mater.* **2021**, *554*, 153068. [CrossRef]

33. Alimov, V.K.; Hatano, Y.; Kuwabara, T.; Toyama, T.; Someya, Y.; Spitsyn, A.V. Deuterium release from deuterium plasma-exposed neutron-irradiated and non-neutron-irradiated tungsten samples during annealing. *Nucl. Fusion* **2020**, *60*, 096025. [CrossRef]

34. AbuAlRoos, N.J.; Azman, M.N.; Amin, N.A.B.; Zainon, R. Tungsten-based material as promising new lead-free gamma radiation shielding material in nuclear medicine. *Phys. Medica* **2020**, *78*, 48–57. [CrossRef] [PubMed]

35. Tanno, T.; Fukuda, M.; Nogami, S.; Hasegawa, A. Microstructure development in neutron irradiated tungsten alloys. *Mater. Trans.* **2011**, *52*, 1447–1451. [CrossRef]

36. He, J.C.; Tang, G.Y.; Hasegawa, A.; Abe, K. Microstructural development and irradiation hardening of W and W–(3–26) wt.% Re alloys after high-temperature neutron irradiation to 0.15 dpa. *Nucl. Fusion* **2006**, *46*, 877. [CrossRef]

37. Klimenkov, M.; Jäntsch, U.; Rieth, M.; Schneider, H.C.; Armstrong, D.E.J.; Gibson, J.S.L.K.; Roberts, S.G. Effect of neutron irradiation on the microstructure of tungsten. *Nucl. Mater. Energy* **2016**, *9*, 480–483. [CrossRef]

38. Bonny, G.; Konstantinovic, M.J.; Bakaeva, A.; Yin, C.; Castin, N.; Mergia, K.; Chatzikos, V.; Dellis, S.; Khvan, T.; Dubinko, A.; et al. Trends in vacancy distribution and hardness of high temperature neutron irradiated single crystal tungsten. *Acta Mater.* **2020**, *198*, 1–9. [CrossRef]

39. Papadakis, D.; Mergia, K.; Manios, E.; Chatzikos, V.; Dellis, S.; Messoloras, S. Post neutron irradiation annealing and defect evolution in single crystal tungsten. *Nucl. Mater. Energy* **2023**, *34*, 101357. [CrossRef]

40. Li, Z.Z.; Li, Y.H.; Terentyev, D.; Castin, N.; Bakaev, A.; Bonny, G.; Yang, Z.; Liang, L.; Zhou, H.-B.; Gao, F.; et al. Investigating the formation mechanism of void lattice in tungsten under neutron irradiation: From collision cascades to ordered nanovoids. *Acta Mater.* **2021**, *219*, 117239. [CrossRef]

41. Mergia, K.; Chatzikos, V.; Manios, E.; Dellis, S.; Papadakis, D.; Terentyev, D.; Bonny, G.; Dubinko, A.; Stamatelatos, I.; Messoloras, S.; et al. Evolution of microstructure in neutron irradiated cold rolled tungsten and its correlation with hardness. *Fusion Engg. Design* **2021**, *172*, 112784. [CrossRef]

42. Yin, C.; Bonny, G.; Terentyev, D. Anisotropy in the hardness of single crystal tungsten before and after neutron irradiation. *J. Nucl. Mater.* **2021**, *546*, 152759. [CrossRef]

43. Oya, Y.; Sun, F.; Yamauchi, Y.; Nobuta, Y.; Shimada, M.; Taylor, C.N.; Wampler, W.; Nakata, M.; Garrison, L.; Hatano, Y. D retention and depth profile behavior for single crystal tungsten with high temperature neutron irradiation. *J. Nucl. Mater.* **2020**, *539*, 152323. [CrossRef]

44. Chatzikos, V.; Mergia, K.; Bonny, G.; Terentyev, D.; Papadakis, D.; Pavlou, G.E.; Messoloras, S. Positron annihilation spectroscopy investigation of defects in neutron irradiated tungsten materials. *Int. J. Refract. Metals Hard Mater.* **2022**, *105*, 105838. [CrossRef]

45. Gietl, H.; Koyanagi, T.; Hu, X.; Fukuda, M.; Hasegawa, A.; Katoh, Y. Neutron irradiation-enhanced grain growth in tungsten and tungsten alloys. *J. Alloys Compd.* **2022**, *901*, 163419. [CrossRef]

46. Hu, X.; Parish, C.M.; Wang, K.; Koyanagi, T.; Eftink, B.P.; Katoh, Y. Transmutation-induced precipitation in tungsten irradiated with a mixed energy neutron spectrum. *Acta Mater.* **2019**, *165*, 51–61. [CrossRef]
47. He, J.C.; Hasegawa, A.; Abe, K. Effects of transmutation elements on the defect structure development of W irradiated by protons and neutrons. *J. Nucl. Mater.* **2008**, *377*, 348–351. [CrossRef]
48. Fukuda, M.; Kumar, N.K.; Koyanagi, T.; Garrison, L.M.; Snead, L.L.; Katoh, Y.; Hasegawa, A. Neutron energy spectrum influence on irradiation hardening and microstructural development of tungsten. *J. Nucl. Mater.* **2016**, *479*, 249–254. [CrossRef]
49. Tanno, T.; Hasegawa, A.; He, J.C.; Fujiwara, M.; Nogami, S.; Satou, M.; Shishido, T.; Abe, K. Effects of transmutation elements on neutron irradiation hardening of tungsten. *Mater. Trans.* **2007**, *48*, 2399–2402. [CrossRef]
50. Xu, A.; Beck, C.; Armstrong, D.E.; Rajan, K.; Smith, G.D.; Bagot, P.A.; Roberts, S.G. Ion-irradiation-induced clustering in W–Re and W–Re–Os alloys: A comparative study using atom probe tomography and nanoindentation measurements. *Acta Mater.* **2015**, *87*, 121–127. [CrossRef]
51. Terentyev, D.; Anento, N.; Serra, A. Interaction of <1 0 0> loops with Carbon atoms and <1 0 0> dislocations in BCC Fe: An atomistic study. *J. Nucl. Mater.* **2012**, *420*, 9–15.
52. Castin, N.; Dwivedi, P.; Messina, L.; Bakaev, A.; Terentyev, D.; Bonny, G. The effect of rhenium on the diffusion of small interstitial clusters in tungsten. *Comput. Mater. Sci.* **2020**, *177*, 109580. [CrossRef]
53. Castin, N.; Bakaev, A.; Terentyev, D.; Pascuet, M.I.; Bonny, G. Understanding why dislocation loops are visible in transmission electron microscopy: The tungsten case. *J. Nucl. Mater.* **2021**, *555*, 153122. [CrossRef]
54. Arakawa, K.; Ono, K.; Isshiki, M.; Mimura, K.; Uchikoshi, M.; Mori, H. Observation of the one-dimensional diffusion of nanometer-sized dislocation loops. *Science* **2007**, *318*, 956–959. [CrossRef]
55. Arakawa, K.; Marinica, M.C.; Fitzgerald, S.; Proville, L.; Nguyen-Manh, D.; Dudarev, S.L.; Ma, P.-W.; Swinburne, T.D.; Goryaeva, A.M.; Amino, T.; et al. Quantum de-trapping and transport of heavy defects in tungsten. *Nat. Mater.* **2020**, *19*, 508–511. [CrossRef]
56. Domain, C.; Becquart, C.S. Solute–<111> interstitial loop interaction in α-Fe: A DFT study. *J. Nucl. Mater.* **2018**, *499*, 582–594.
57. Castin, N.; Bonny, G.; Bakaev, A.; Bergner, F.; Domain, C.; Hyde, J.M.; Radiguet, B.; Malerba, L. The dominant mechanisms for the formation of solute-rich clusters in low-Cu steels under irradiation. *Mater. Today Energy* **2020**, *17*, 100472. [CrossRef]
58. Fukuda, M.; Yabuuchi, K.; Nogami, S.; Hasegawa, A.; Tanaka, T. Microstructural development of tungsten and tungsten–rhenium alloys due to neutron irradiation in HFIR. *J. Nucl. Mater.* **2014**, *455*, 460–463. [CrossRef]
59. Fukuda, M.; Tanno, T.; Nogami, S.; Hasegawa, A. Effects of Re content and fabrication process on microstructural changes and hardening in neutron irradiated tungsten. *Mater. Trans.* **2012**, *53*, 2145–2150. [CrossRef]
60. Hasegawa, A.; Fukuda, M.; Nogami, S.; Yabuuchi, K. Neutron irradiation effects on tungsten materials. *Fusion Eng. Des.* **2014**, *89*, 1568–1572. [CrossRef]
61. Hwang, T.; Hasegawa, A.; Tomura, K.; Ebisawa, N.; Toyama, T.; Nagai, Y.; Fukuda, M.; Miyazawa, T.; Tanaka, T.; Nogami, S. Effect of neutron irradiation on rhenium cluster formation in tungsten and tungsten-rhenium alloys. *J. Nucl. Mater.* **2018**, *507*, 78–86. [CrossRef]
62. Hasegawa, A.; Fukuda, M.; Yabuuchi, K.; Nogami, S. Neutron irradiation effects on the microstructural development of tungsten and tungsten alloys. *J. Nucl. Mater.* **2016**, *471*, 175–183. [CrossRef]
63. Vesti, A.; Music, D.; Olsson, P.A. First-principles study on thermal expansion of W-Re sigma and chi phases. *Nucl. Mater. Energy* **2024**, *39*, 101684. [CrossRef]
64. Suzudo, T.; Yamaguchi, M.; Hasegawa, A. Stability and mobility of rhenium and osmium in tungsten: First principles study. *Model. Simul Mat. Sci. Eng.* **2014**, *22*, 075006. [CrossRef]
65. Huang, C.H.; Gharaee, L.; Zhao, Y.; Erhart, P.; Marian, J. Mechanism of nucleation and incipient growth of Re clusters in irradiated W-Re alloys from kinetic Monte Carlo simulations. *Phys. Rev. B* **2017**, *96*, 094108. [CrossRef]
66. Massalski, T.B.; Okamoto, H.; Subramanian, P.; Kacprzak, L.; Scott, W.W. *Binary Alloy Phase Diagrams (Vol. 1, No. 2)*; American Society for Metals: Metals Park, OH, USA, 1986.
67. Berne, C.; Sluiter, M.; Kawazoe, Y.; Hansen, T.; Pasturel, A. Site occupancy in the Re-W sigma phase. *Phys. Rev. B* **2001**, *64*, 144103. [CrossRef]
68. Crivello, J.C.; Breidi, A.; Joubert, J.M. χ and σ phases in binary rhenium–transition metal systems: A systematic first-principles investigation. *Inorg. Chem.* **2013**, *52*, 3674–3686. [CrossRef]
69. Bonny, G.; Bakaev, A.; Terentyev, D.; Mastrikov, Y.A. Elastic properties of the sigma W-Re phase: A first principles investigation. *Scr. Mater.* **2017**, *128*, 45–48. [CrossRef]
70. Vesti, A.; Hiremath, P.; Melin, S.; Olsson, P.A. Ab-initio investigation of mechanical and fracture-related properties of W-Re σ and χ precipitates. *J. Nucl. Mater.* **2023**, *577*, 154261. [CrossRef]
71. Harrison, R.W.; Greaves, G.; Hinks, J.A.; Donnelly, S.E. Intermetallic Re phases formed in ion irradiated WRe alloy. *J. Nucl. Mater.* **2019**, *514*, 123–127. [CrossRef]
72. Setyawan, W.; Nandipati, G.; Roche, K.J.; Heinisch, H.L.; Wirth, B.D.; Kurtz, R.J. Displacement cascades and defects annealing in tungsten, Part I: Defect database from molecular dynamics simulations. *J. Nucl. Mater.* **2015**, *462*, 329–337. [CrossRef]
73. Nandipati, G.; Setyawan, W.; Heinisch, H.L.; Roche, K.J.; Kurtz, R.J.; Wirth, B.D. Displacement cascades and defect annealing in tungsten, Part II: Object kinetic Monte Carlo simulation of tungsten cascade aging. *J. Nucl. Mater.* **2015**, *462*, 338–344. [CrossRef]
74. Wróbel, J.S.; Nguyen-Manh, D.; Kurzydłowski, K.J.; Dudarev, S.L. A first-principles model for anomalous segregation in dilute ternary tungsten-rhenium-vacancy alloys. *J. Phys. Condens. Matter.* **2017**, *29*, 145403. [CrossRef]

75. Li, Y.H.; Zhou, H.B.; Deng, H.; Lu, G.; Lu, G.H. Towards understanding the mechanism of rhenium and osmium precipitation in tungsten and its implication for tungsten-based alloys. *J. Nucl. Mater.* **2018**, *505*, 30–43. [CrossRef]

76. Lloyd, M.J.; Abernethy, R.G.; Gilbert, M.R.; Griffiths, I.; Bagot, P.A.; Nguyen-Manh, D.; Moody, M.P.; Armstrong, D.E. Decoration of voids with rhenium and osmium transmutation products in neutron irradiated single crystal tungsten. *Scr. Mater.* **2019**, *173*, 96–100. [CrossRef]

77. Hu, X.; Koyanagi, T.; Fukuda, M.; Kumar, N.K.; Snead, L.L.; Wirth, B.D.; Katoh, Y. Irradiation hardening of pure tungsten exposed to neutron irradiation. *J. Nucl. Mater.* **2016**, *480*, 235–243. [CrossRef]

78. Tanno, T.; Hasegawa, A.; Fujiwara, M.; He, J.C.; Nogami, S.; Satou, M.; Shishido, T.; Abe, K. Precipitation of solid transmutation elements in irradiated tungsten alloys. *Mater. Trans.* **2008**, *49*, 2259–2264. [CrossRef]

79. Hasegawa, A.; Fukuda, M.; Tanno, T.; Nogami, S. Neutron irradiation behavior of tungsten. *Mater. Trans.* **2013**, *54*, 466–471. [CrossRef]

80. Yi, X.; Jenkins, M.L.; Hattar, K.; Edmondson, P.D.; Roberts, S.G. Characterization of radiation damage in W and W-based alloys from 2 MeV self-ion near-bulk implantations. *Acta Mater.* **2015**, *92*, 163–177. [CrossRef]

81. Van Renterghem, W.; Uytdenhouwen, I. Investigation of the combined effect of neutron irradiation and electron beam exposure on pure tungsten. *J. Nucl. Mater.* **2016**, *477*, 77–84. [CrossRef]

82. Sikka, V.K.; Moteff, J. "Rafting" in neutron irradiated tungsten. *J. Nucl. Mater.* **1973**, *46*, 217–219. [CrossRef]

83. Li, M.; Eldrup, M.; Byun, T.S.; Hashimoto, N.; Snead, L.L.; Zinkle, S.J. Low temperature neutron irradiation effects on microstructure and tensile properties of molybdenum. *J. Nucl. Mater.* **2008**, *376*, 11–28. [CrossRef]

84. Dürrschnabel, M.; Klimenkov, M.; Jäntsch, U.; Rieth, M.; Schneider, H.C.; Terentyev, D. New insights into microstructure of neutron-irradiated tungsten. *Sci. Rep.* **2021**, *11*, 7572. [CrossRef] [PubMed]

85. Lloyd, M.J.; Haley, J.; Jim, B.; Abernethy, R.; Gilbert, M.R.; Martinez, E.; Hattar, K.; El-Atwani, O.; Nguyen-Manh, D.; Moody, M.P.; et al. Microstructural evolution and transmutation in tungsten under ion and neutron irradiation. *Materialia* **2024**, *33*, 101991. [CrossRef]

86. Van Renterghem, W.; Bonny, G.; Terentyev, D. TEM investigation of neutron irradiated and post irradiation annealed tungsten materials. *Fusion Eng. Des.* **2022**, *180*, 113170. [CrossRef]

87. Cetiner, N.O.; Hatano, Y.; McDuffee, J.L.; Ilas, D.; Katoh, Y.; Geringer, J.W.; Toyama, T. Neutron irradiation of tungsten in hydrogen environment at HFIR. *Fusion Eng. Des.* **2022**, *178*, 113089. [CrossRef]

88. Muroga, T.; Hatano, Y.; Clark, D.; Katoh, Y. Characterization and qualification of neutron radiation effects–Summary of Japan-USA Joint Projects for 40 years. *J. Nucl Mater.* **2022**, *560*, 153494. [CrossRef]

89. Miyazawa, T.; Garrison, L.M.; Geringer, J.W.; Echols, J.R.; Fukuda, M.; Katoh, Y.; Hinoki, T.; Hasegawa, A. Tensile properties of powder-metallurgical-processed tungsten alloys after neutron irradiation near recrystallization temperatures. *J. Nucl. Mater.* **2020**, *542*, 152505. [CrossRef]

90. Miyazawa, T.; Garrison, L.M.; Geringer, J.W.; Fukuda, M.; Katoh, Y.; Hinoki, T.; Hasegawa, A. Neutron irradiation effects on the mechanical properties of powder metallurgical processed tungsten alloys. *J. Nucl. Mater.* **2020**, *529*, 151910. [CrossRef]

91. Tanoue, Y.; Yokoyama, T.; Ozawa, M. Feasibility Study on Production of High-Purity Rhenium-185 by Nuclear Transmutation of Natural Tantalum. *J. Nucl. Eng.* **2023**, *4*, 625–633. [CrossRef]

92. Nogami, S.; Hasegawa, A.; Fukuda, M.; Rieth, M.; Reiser, J.; Pintsuk, G. Mechanical properties of tungsten: Recent research on modified tungsten materials in Japan. *J. Nucl. Mater.* **2021**, *543*, 152506. [CrossRef]

93. Watanabe, S.; Nogami, S.; Reiser, J.; Rieth, M.; Sickinger, S.; Baumgärtner, S.; Miyazawa, T.; Hasegawa, A. Tensile and impact properties of tungsten-rhenium alloy for plasma-facing components in fusion reactor. *Fusion Eng. Des.* **2019**, *148*, 111323. [CrossRef]

94. Roth, J.; Tsitrone, E.; Loarte, A.; Loarer, T.; Counsell, G.; Neu, R.; Philipps, V.; Brezinsek, S.; Lehnen, M.; Coad, P.; et al. Recent analysis of key plasma wall interactions issues for ITER. *J. Nucl. Mater.* **2009**, *390*, 1–9. [CrossRef]

95. Anand, M.S.; Pande, B.M.; Agarwala, R.P. Recovery in neutron irradiated tungsten. *Radiat. Eff.* **1978**, *39*, 149–155. [CrossRef]

96. Garrison, L.M.; Katoh, Y.; Geringer, J.W.; Akiyoshi, M.; Chen, X.; Fukuda, M.; Hasegawa, A.; Hinoki, T.; Hu, X.; Koyanagi, T.; et al. Phenix US-Japan collaboration investigation of thermal and mechanical properties of thermal neutron–shielded irradiated tungsten. *Fusion Sci. Technol.* **2019**, *75*, 499–509. [CrossRef]

97. Gaganidze, E.; Chauhan, A.; Schneider, H.C.; Terentyev, D.; Borghmans, G.; Aktaa, J. Fracture-mechanical properties of neutron irradiated ITER specification tungsten. *J. Nucl. Mater.* **2021**, *547*, 152761. [CrossRef]

98. Gilbert, M.R.; Dudarev, S.L.; Nguyen-Manh, D.; Zheng, S.; Packer, L.W.; Sublet, J.C. Neutron-induced dpa, transmutations, gas production, and helium embrittlement of fusion materials. *J. Nucl. Mater.* **2013**, *442*, S755–S760. [CrossRef]

99. Papadakis, D.; Dellis, S.; Chatzikos, V.; Manios, E.; Stamatelatos, I.E.; Messoloras, S.; Mergia, K. Neutron irradiation effects in different tungsten microstructures. *Phys. Scr.* **2021**, *96*, 124041. [CrossRef]

100. Yi, X.; Jenkins, M.L.; Briceno, M.; Roberts, S.G.; Zhou, Z.; Kirk, M.A. In situ study of self-ion irradiation damage in W and W–5Re at 500 C. *Phil. Mag.* **2013**, *93*, 1715–1738. [CrossRef]

101. Field, K.G.; Hu, X.; Littrell, K.C.; Yamamoto, Y.; Snead, L.L. Radiation tolerance of neutron-irradiated model Fe–Cr–Al alloys. *J. Nucl. Mater.* **2015**, *465*, 746–755. [CrossRef]

102. Parish, C.M.; Wang, K.; Edmondson, P.D. Nanoscale chemistry and crystallography are both the obstacle and pathway to advanced radiation-tolerant materials. *Scr. Mater.* **2018**, *143*, 169–175. [CrossRef]

103. Ralph, B.; Brandon, D.G. A field ion microscope study of some tungsten-rhenium alloys. *Phil. Mag.* **1963**, *8*, 919–934. [CrossRef]
104. Edmondson, P.D.; Gault, B.; Gilbert, M.R. An atom probe tomography and inventory calculation examination of second phase precipitates in neutron irradiated single crystal tungsten. *Nucl. Fusion* **2020**, *60*, 126013. [CrossRef]
105. Akiyoshi, M.; Garrison, L.M.; Geringer, J.W.; Wang, H.; Hasegawa, A.; Nogami, S.; Katoh, Y. Thermal diffusivity of irradiated tungsten and tungsten-rhenium alloys. *J. Nucl. Mater.* **2021**, *543*, 152594. [CrossRef]
106. Tanabe, T.; Eamchotchawalit, C.; Busabok, C.; Taweethavorn, S.; Fujitsuka, M.; Shikama, T. Temperature dependence of thermal conductivity in W and W–Re alloys from 300 to 1000 K. *Mater. Lett.* **2003**, *57*, 2950–2953. [CrossRef]
107. Terentyev, D.; Yin, C.; Dubinko, A.; Chang, C.C.; You, J.H. Neutron irradiation hardening across ITER diverter tungsten armor. *Int. J. Refract. Hard Mater.* **2021**, *95*, 105437. [CrossRef]
108. Huang, C.H.; Gilbert, M.R.; Marian, J. Simulating irradiation hardening in tungsten under fast neutron irradiation including Re production by transmutation. *J. Nucl. Mater.* **2018**, *499*, 204–215. [CrossRef]
109. Garrison, L.M.; Katoh, Y.; Kumar, N.K. Mechanical properties of single-crystal tungsten irradiated in a mixed spectrum fission reactor. *J. Nucl. Mater.* **2019**, *518*, 208–225. [CrossRef]
110. Yin, C.; Terentyev, D.; Pardoen, T.; Petrov, R.; Tong, Z. Ductile to brittle transition in ITER specification tungsten assessed by combined fracture toughness and bending tests analysis. *Mater. Sci. Eng. A* **2019**, *750*, 20–30. [CrossRef]
111. Yin, C.; Terentyev, D.; Zhang, T.; Petrov, R.H.; Pardoen, T. Impact of neutron irradiation on the strength and ductility of pure and ZrC reinforced tungsten grades. *J. Nucl. Mater.* **2020**, *537*, 152226. [CrossRef]
112. Nobuta, Y.; Shimada, M.; Taylor, C.N.; Oya, Y.; Hatano, Y.; Wu, Y.; Dubey, M. Effects of helium seeding on deuterium retention in neutron-irradiated tungsten. *Fusion Sci. Technol.* **2021**, *77*, 76–79. [CrossRef]
113. Oya, Y.; Hatano, Y.; Shimada, M.; Buchenauer, D.; Kolasinski, R.; Merrill, B.; Kondo, S.; Hinoki, T.; Alimov, V.K. Recent progress of hydrogen isotope behavior studies for neutron or heavy ion damaged, W. *Fusion Sci. Technol.* **2016**, *113*, 211–215. [CrossRef]
114. Gilbert, M.R.; Arakawa, K.; Bergstrom, Z.; Caturla, M.J.; Dudarev, S.L.; Gao, F.; Goryaeva, A.; Hu, S.; Hu, X.; Kurtz, R.; et al. Perspectives on multiscale modelling and experiments to accelerate materials development for fusion. *J. Nucl. Mater.* **2021**, *554*, 153113. [CrossRef]
115. Field, K.G.; Briggs, S.A.; Hu, X.; Yamamoto, Y.; Howard, R.H.; Sridharan, K. Heterogeneous dislocation loop formation near grain boundaries in a neutron-irradiated commercial FeCrAl alloy. *J. Nucl. Mater.* **2017**, *483*, 54–61. [CrossRef]
116. Linke, J. Plasma facing materials and components for future fusion devices—Development, characterization and performance under fusion specific loading conditions. *Phys. Scr.* **2006**, *T123*, 45. [CrossRef]
117. Raffray, A.R.; Nygren, R.; Whyte, D.G.; Abdel-Khalik, S.; Doerner, R.; Escourbiac, F.; Evans, T.; Goldston, R.J.; Hoelzer, D.T.; Konishi, S.; et al. High heat flux components—Readiness to proceed from near term fusion systems to power plants. *Fusion Eng. Des.* **2010**, *85*, 93–108. [CrossRef]
118. Savitskii, E.M.; Tylkina, M.A.; Ipatova, S.I.; Pavlova, E.I. Properties of tungsten-rhenium alloys. *Met. Sci. Heat Treat. Met.* **1960**, *2*, 483–486. [CrossRef]
119. Klopp, W.D. A review of chromium, molybdenum, and tungsten alloys. *J. Less Common Met.* **1975**, *42*, 261–278. [CrossRef]
120. Greenwood, L.R.; Garner, F.A. Transmutation of Mo, Re, W, Hf, and V in various irradiation test facilities and STARFIRE. *J. Nucl. Mater.* **1994**, *212*, 635–639. [CrossRef]
121. Armstrong, D.E.J.; Yi, X.; Marquis, E.A.; Roberts, S.G. Hardening of self-ion implanted tungsten and tungsten 5-wt% rhenium. *J. Nucl. Mater.* **2013**, *432*, 428–436. [CrossRef]
122. Cottrell, G.A.; Pampin, R.; Taylor, N.P. Transmutation and phase stability of tungsten armor in fusion power plants. *Fusion Sci. Technol.* **2006**, *50*, 89–98. [CrossRef]
123. Wirth, B.D.; Odette, G.R.; Marian, J.; Ventelon, L.; Young-Vandersall, J.A.; Zepeda-Ruiz, L.A. Multiscale modeling of radiation damage in Fe-based alloys in the fusion environment. *J. Nucl. Mater.* **2004**, *329*, 103–111. [CrossRef]
124. Neu, R.; Bobkov, V.; Dux, R.; Kallenbach, A.; Pütterich, T.; Greuner, H.; Gruber, O.; Herrmann, A.; Hopf, C.; Krieger, K.; et al. Final steps to an all tungsten divertor tokamak. *J. Nucl. Mater.* **2007**, *363*, 52–59. [CrossRef]
125. Campbell, A.A.; Porter, W.D.; Katoh, Y.; Snead, L.L. Method for analyzing passive silicon carbide thermometry with a continuous dilatometer to determine irradiation temperature. *Nucl. Instru. Methods Phys. Res. Sect. B Beam Interact. Mater. At.* **2016**, *370*, 49–58. [CrossRef]
126. Balluffi, R.W. Vacancy defect mobilities and binding energies obtained from annealing studies. *J. Nucl. Mater.* **1978**, *69*, 240–263. [CrossRef]
127. Mundy, J.N.; Ockers, S.T.; Smedskjaer, L.C. Vacancy migration enthalpy in tungsten at high temperatures. *Phil. Mag. A* **1987**, *56*, 851–860. [CrossRef]
128. Xiao, X.; Terentyev, D.; Chu, H.; Duan, H. Theoretical models for irradiation hardening and embrittlement in nuclear structural materials: A review and perspective. *Acta Mech. Sin.* **2020**, *36*, 397–411. [CrossRef]
129. Dellis, S.; Xiao, X.; Terentyev, D.; Manios, E.; Mergia, K. Hardening mechanisms of "cold" rolled tungsten after neutron irradiation: Indentation and finite elements modelling. *Int. J. Refract. Met. Hard Mater.* **2023**, *111*, 106096. [CrossRef]